LBL-5123
c.1

CHEMICAL APPLICATIONS OF X-RAY PHOTOELECTRON SPECTROSCOPY

Bernice Elizabeth Mills
(Ph. D. thesis)

May 1976

Prepared for the U. S. Energy Research and Development Administration under Contract W-7405-ENG-48

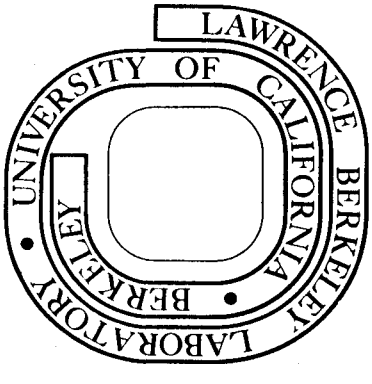

LBL-5123
c.1

DISCLAIMER

CHEMICAL APPLICATIONS OF X-RAY PHOTOELECTRON SPECTROSCOPY

Contents

ABSTRACT vii

INTRODUCTION 1

References 5

I. A COMPARISON OF VALENCE SHELL AND CORE IONIZATION POTENTIALS OF ALKYL IODIDES 6

Abstract 6

Introduction 7

Experimental 7

Results and Discussion 8

Table 11

References 12

Figures 13

II. STUDIES OF THE CORE BINDING ENERGY — PROTON AFFINITY CORRELATION IN MOLECULES 16

Abstract 16

Introduction 17

Experimental 19

Results 19

Discussion 20

Conclusions 29

References 31

Table 33

Figures 35

III. X-RAY PHOTOEMISSION MOLECULAR ORBITALS OF HYDROGEN FLUORIDE AND THE FLUORINATED METHANES 40
Abstract 40
Introduction 41
Experimental 43
Orbital Binding Energies 44
Intensities and Spectroscopic Assignments 50
Trends Through the Series 54
References 56
Tables 58
Figures 64
IV. XPS OF THE 2s REGION OF CYCLIC HYDROCARBONS IN RELATION TO AMORPHOUS GROUP IV AND V ELEMENTS 69
Abstract 69
Introduction 70
Experimental 72
Theoretical 74
Results and Discussion 76
References 79
Table 81
Figures 83
V. THE FLUORINE 1s CORRELATION-STATE ("SHAKE-UP") SPECTRUM IN THE PHOTOIONIZATION OF HYDROGEN FLUORIDE 88
Abstract 88
Introduction 89
Experimental 90

Conclusions 93

References 98

Table 99

Figures 100

VI. K-SHELL CORRELATION-STATE ("SHAKE-UP") SPECTRA IN FORMAMIDE .. 104

Abstract 104

References 111

Table 112

Figures 113

ACKNOWLEDGEMENTS 116

CHEMICAL APPLICATIONS OF X-RAY PHOTOELECTRON SPECTROSCOPY

Bernice Elizabeth Mills

Materials and Molecular Research Division
Lawrence Berkeley Laboratory
and
Department of Chemistry
University of California
Berkeley, California 94720

ABSTRACT

X-ray photoelectron spectroscopy was used to study the effect of chemical environment and molecular structure on the electronic levels of various free molecules and elemental solids.

Core level binding energies were measured and compared with first ionization potentials in a series of alkyl iodides in order to understand the effect of changes in substituent on the electron density around the iodine nucleus. Core level binding-energy shifts were measured for oxygen 1s levels in alcohols, ethers, aldehydes, acids, esters, and acetone; nitrogen 1s levels in ammonia and aliphatic amines; phosphorus 2p levels in phosphine and its methyl derivatives; and sulfur 2p levels in H_2S and its methyl derivatives. These shifts were found to correlate well with proton affinities. Fine structure was clearly visible in the case of the amines indicating slightly different effects of methyl substitution and chain lengthening. The latter reflects the response of the system to long range effects, while the former results from changes in the local bonds.

The molecular orbitals of methane, hydrogen fluoride, and the series of fluorinated methanes were studied. Excellent prediction of orbital energies from ab initio Koopmans' theorem energies was possible using a three parameter model. The use of orbital intensities derived from net populations from CNDO/2 or ab initio calculations enabled the clarification of certain questions about level-ordering. The valence spectra of some cyclic alkanes were taken in order to find the cause of an interesting effect in the spectrum of amorphous tetrahedrally-bonded group IV and V elements, as compared with the corresponding crystalline spectra. The effects is apparently the result of the inclusion of odd-membered rings in the structure of the amorphous elements.

"Shake-up" lines in the fluorine 1s spectrum of hydrogen fluoride were studied for comparison with theory. These states can be thought of as arising from configuration interaction (CI) in many-electron theory in both the ground and excited states, and the rearrangement of electron density upon core ionization. When using CI in both the ground and excited states, excellent agreement was obtained between the calculated and observed intensities. Similar spectra were obtained for the 1s levels of carbon, nitrogen, and oxygen in formamide ($HCONH_2$) and compared to less detailed predictions by Bash. This prototypical study, with 1s holes on three different elements in the same molecule, shows that $\pi \rightarrow \pi^*$ excitations are differentially stabilized according to the location of the 1s hole.

INTRODUCTION

X-ray photoelectron spectroscopy (XPS or ESCA, for Electron Spectroscopy for Chemical Analysis) has begun, in the last few years, to fulfill some of its promise as a spectroscopic method for the study of a wide range of systems. As such, it has been the subject of several excellent books and review articles[1-6] and needs little introduction. The spectrometer used in this work, the 50 cm Berkeley iron-free magnetic spectrometer, has also been described in detail elsewhere.[7,8]

The technique of XPS will be described briefly here for those who have not read the books and review articles. A mono-energetic beam of x-rays (e.g. the characteristic lines of aluminum or magnesium) is used to irradiate a sample, ejecting photoelectrons. These electrons are then energy-analyzed to give a spectrum of intensity (number of electrons counted) vs. kinetic energy (KE). The energy scale of the spectrum is usually changed using the relationship

$$E_B = h\nu - KE \quad ,$$

where E_B is the binding energy of the electron and $h\nu$ is the energy of the x-ray photon (all are expressed in electron volts, eV). Since the spectra are originally taken vs. KE, they are customarily displayed with the binding energy scale increasing to the left.

To a first approximation a photoelectron spectrum can be considered a map in energy space of the electronic levels of a system. It shows the valence levels, molecular orbitals, or bands of atoms,

molecules, or solids, respectively. In addition each atom of $Z \geq 3$ has at least one core level, and these levels are basically atomic in character no matter what the chemical environment.

On a finer scale there are six types of features seen in an XPS spectrum. The first three types will not be discussed in detail in this thesis, but will be mentioned here for completeness. First, with a spectrometer like that used in this work (and most others) the x-ray source is not completely monochromatic. It addition to a background of continuum radiation, unmonochromatized characteristic x-rays have satellites the largest of which, in this case, are about 10 eV from the main line and have an intensity of about 10% of the main line. They can usually be corrected for easily. Secondly, we see Auger electrons. These are caused by "radiationless" decay of an ion with a hole in an inner shell. When an electron from another level falls into the hole, the system, instead of emitting an x-ray, emits an electron which carries off the excess energy. Auger energies are, of course, independent of the energy of the exciting radiation and if necessary the Auger lines can be determined by changing the characteristic x-ray line used. This is not usually needed, though, for the same reason that it is usually no problem to know which level of which element gives rise to a given XPS peak--the levels are separated by vast deserts of empty energy space, much as NMR levels for different nuclei are separated. Thirdly, we see electrons which came from specific energy levels but suffered an inelastic collision before reaching the slit to the energy analyzer. They therefore appear as a peak at a lower kinetic energy than the main line.

In gases these collisions might excite a molecule to a higher electronic state, in solids they might cause excitation of a phonon mode. It is possible to obtain information from these loss peaks, and it is also necessary to take them into consideration if they may interfere with another process under study. In gas-phase work, the primary subject of this thesis, these levels can be identified by their enhancement at high pressures.

In Chapters I and II we discuss examples of structural and electronic information that can be obtained from core-level binding energy chemical shifts. These chemical shifts arise from the effect on the binding energy of differences in ground state charge distribution and final (hole) state electron rearrangement or relaxation. The first is related to the inductive effect of substituents and the second to their polarizability. By comparing binding energy shifts to other measurements (in this case first ionization potentials and proton affinities), we can obtain information about the electronic structure of molecules.

The next two chapters deal with molecular-orbital spectra and are examples of the kinds of information that can be obtained from them. Molecular orbitals are not, of course, very atomic in character. Their intensities, however, are highly dependent on the atomic orbital character of the molecular orbital. In addition the most tightly bound molecular orbitals reflect the local bonding symmetry of the system. Both of the effects are discussed in Chapters III and IV.

Chapters V and VI deal with the treatment of "shake-up" spectra. These spectra are actually satellites on the low kinetic energy

(high binding energy) side of "ordinary" photoelectron peaks. They are commonly explained as arising from simultaneous ejection of a photoelectron and excitation of a valence electron into an unfilled valence level, hence the name shake-up. Predictions based on this model are, at this time, so poor as to be of little use in the understanding and interpretation of most shake-up spectra. Theoretical calculations are necessary. A very sophisticated calculation has been performed on hydrogen fluoride F 1s and is compared with the experimental spectrum in Chapter V. Chapter VI presents the carbon, nitrogen, and oxygen 1s shake-up spectra of formamide and compares them to some less rigorous predictions.

References

1. K. Siegbahn, C. Nordling, A. Fahlman, R. Nordberg, K. Hamrin, J. Hedman, G. Johansson, T. Bergmark, S.-E. Karlsson, I. Lindgren, and B. J. Lindberg, ESCA - Atomic, Molecular, and Solid State Structure by Means of Electron Spectroscopy, Nova Acta Regiae Soc. Sci. Upsaliensis Ser. IV, Vol. 20 (1967).

2. K. Siegbahn, C. Nordling, G. Johansson, J. Hedman, P. F. Hedén, K. Hamrin, U. Gelius, T. Bergmark, L. O. Werme, R. Manne, and Y. Baer, ESCA Applied to Free Molecules, North-Holland Publishing Co., Amsterdam, 1969.

3. D. A. Shirley, editor, "Electron Spectroscopy", (North-Holland, 1972).

4. D. A. Shirley, Adv. Chem. Phys. 23, 85 (1973).

5. W. L. Jolly, Coord. Rev. 13, 47 (1974).

6. T. A. Carlson, Ann. Phys. Chem. 26, 211 (1975).

7. K. Siegbahn in Alpha-, Beta-, and Gamma-Ray Spectroscopy, K. Siegbahn, Ed., (North-Holland Publishing Co., Amsterdam, 1965) Vol. 1, Ch. III. 5.

8. C. S. Fadley, "Core and Valence Electronic States Studied with X-ray Photoelectron Spectroscopy" (Ph.D. Thesis), Lawrence Radiation Laboratory Report UCRL-19535 (1970), and references therein.

I. A COMPARISON OF VALENCE SHELL AND CORE IONIZATION POTENTIALS OF ALKYL IODIDES

Abstract

X-ray photoelectron spectroscopy was used to study the relative ionization potentials of the iodine $3d_{5/2}$ level in a series of alkyl iodides and HI. Comparison of these data with the corresponding iodine $5p_{1/2}$ ionization potentials obtained from uv photoelectron spectroscopy established that the chemical shifts are probably due to variations in the electron distribution along the carbon-iodine bond and that the $5p_{1/2}$ level is destabilized at least 0.14 eV by hyperconjugation.

Introduction

It has recently been shown that the valence shell n lone pair ionization potentials of alkyl iodides, bromides, and chlorides correlate well with Taft's σ^* values (as used with the Hammett equation)[1] and even better with each other.[2] Similar correlations have been found between the iodide ionization potentials and those of a series of other alkyl-substituted groups.[3] We now report the $3d_{5/2}$ ionization potential of a series of alkyl iodides. These results are compared with the valence shell ionization potentials to elucidate the probable cause of the chemical shifts and the magnitude of hyperconjugation in these compounds.

Experimental Section

The alkyl iodides are commercially available and were used without further purification.

The $3d_{5/2}$ binding energies were obtained using an x-ray photoelectron spectrometer which has been described previously in detail.[4] A mixture of the sample and the trifluoromethyl iodide used as the reference was introduced into the target chamber and irradiated with Mg Kα x-rays. The resulting spectra of the mixtures were well resolved, and the relative position of the sample peak was determined in each case by a least-squares fit of the two peaks with Gaussian functions. In the case of hydrogen iodide, isopropyl iodide was used as a reference, but the tabulated shift is given relative to trifluoromethyl iodide.

The $3d_{5/2}$ peak was characterized in the usual way by its position and spin-orbit splitting from the $3d_{3/2}$; it was chosen as a representative core level simply because it gives a relatively intense spectrum.

The resulting $3d_{5/2}$ binding energies are summarized in Table I as chemical shifts relative to trifluoromethyl iodide. Table I also includes a summary of the iodine lone pair $5p_{1/2}$ ionization potentials from Ref. 2.

Results and Discussion

A plot of the iodine $5p_{1/2}$ ionization potentials against the corresponding $3d_{5/2}$ chemical shifts is shown in Fig. 1. The linear correlation for the alkyl iodide results contains two significant features that demand explanation. The least-squares line shown in Fig. 1 has a slope, 1.22 ± 0.05, that is *greater* than unity and the point for hydrogen iodide falls off the line. The latter feature is significant because the hydrogen halides fit the corresponding interhalogen correlations given in Ref. 2.

Ionization potentials of various types are known to be responsive toward various measures of substituent behavior--inductive effects in the ground state, polarization (relaxation) effects in the final state. What is surprising, at least at first sight, is that the valence shell lone pair $5p_{1/2}$ ionization potential of iodine is *less responsive* to substituent change than is the core $3d_{5/2}$ ionization potential as given by the slope in Fig. 1. We rationalize this result in the following way. A through-bond inductive or polarization effect can be viewed as a shift of the electrons along the axis of the R-I bond. The electrons in this bond are, on the average, closer to the core atomic orbitals than to the valence shell non-bonding p atomic orbitals and consequently affect them more. This geometrical relation is illustrated in Fig. 2.

This qualitative approach can be cast into more conventional MO language. The R-I bond can be written as a two-center MO made up of an approximately sp^3 hybrid orbital on carbon, ϕ_C, and a predominantly $5p_z$ orbital of iodine, ϕ_I:

$$\psi_{R-I} = a\phi_C + b\phi_I \quad .$$

The incorporation of some contribution from other iodine orbitals will not affect the argument to follow. A substituent on carbon will alter the coefficients, a and b, and the replusion terms with other iodine electrons. From the relative distances involved, repulsion of other iodine electrons to the iodine fraction, b^2, of the R-I bond electrons will be more important than that with the carbon fraction, a^2. However, electron repulsion between electrons in different 5p orbitals is less than that between 5p and any core orbital. For example, in Hartree-Fock calculations on the iodine atom, the Coulomb repulsion integral between 5p electrons in different orbitals is

$$(5p_x 5p_x / 5p_z 5p_z) = 0.69 \text{ Rydberg} \quad ,$$

whereas that for the interaction between a 5p electron and a 3d electron is

$$(3d_i 3d_i / 5p_z 5p_z) = 0.99 \text{ Rydberg} \quad .^5$$

This relationship is appropriate for both the initial and final states.

The displacement of the point for hydrogen iodide from the alkyl iodide correlation line is plausibly explained by hyperconjugation. The iodine 5p levels are destabilized by interaction with appropriate

σ orbitals on the alkyl group (hyperconjugation). This destabilization is partially offset by a stabilizing interaction with the corresponding σ* orbitals (anionic hyperconjugation or backbonding). The core 3d levels are not affected by such interactions and provide a calibration for assessing the magnitude of the hyperconjugation effect; that is, the effect of structural change on the ionization potentials is dissected into an inductive and a conjugative effect. Only the former affects the core levels, whereas both contribute to the lone pair 5p levels. Hydrogen iodide, on the other hand, cannot contain hyperconjugative interactions. The displacement of this point from the line in Fig. 1 thus indicates an average value of 0.14 eV for the hyperconjugative destabilization of iodine $5p_{1/2}$ electrons by alkyl groups. This relatively small effect is similar in magnitude to values calculated by Brogli and Heilbronner[6] using perturbation theory. This value should be taken as a lower bound to the destabilization because relaxation should affect the alkyl iodide 3d more than it affects either the corresponding 5p or the HI 3d. The HI 5p should be least affected by relaxation. There is the further implication in the fit of all the alkyl iodides to a single line that the hyperconjugative interaction with C-C bonds must be approximately the same as with C-H bonds.

The present example demonstrates the unique advantages of using both valence shell and core photoelectron spectroscopy to elucidate the causes for chemical shifts of ionization potentials.

Table I. Summary of the Iodine $5p_{1/2}$ Binding Energies and Relative $3d_{5/2}$ Binding Energies for Alkyl Iodides.

R in RI	$5p_{1/2}$ Binding Energy,[a] eV	$3d_{5/2}$ -Chemical Shift,[b] eV
Methyl	10.14	1.10 ± 0.03
Ethyl	9.93	1.36 ± 0.03
n-Propyl	9.83	1.45 ± 0.04
n-Butyl	9.81	1.49 ± 0.04
n-Pentyl	9.78	1.51 ± 0.03
i-Propyl	9.75	1.57 ± 0.03
t-Butyl	9.64	1.73 ± 0.05
Hydrogen	11.05	0.20 ± 0.04

[a] All errors ± 0.02 eV.

[b] Relative to trifluoromethyl iodide.

References

1. R. W. Taft, Steric Effects in Organic Chemistry, M. S. Newman, Ed., Wiley, New York, 1956, Chapter 13.
2. F. Brogli, J. A. Hashmall, and E. Heilbronner, Helv. Chim. Acta, in press.
3. B. J. Cocksey, J. H. D. Eland, and C. J. Danby, J. Chem. Soc. B, 790 (1971).
4. C. S. Fadely, S. B. M. Hagstrom, M. D. Klein, and D. A. Shirley, J. Chem. Phys. 48 (8), 3779 (1968).
5. These numbers were calculated from the iodine atom results of J. B. Mann, "Atomic Structure Calculations I. Hartree-Fock Energy Results for the Elements Hydrogen to Lawrencium," LA-3690, TID-4500. The 3d-5p repulsions will depend, of course, on the specific d orbitals used but the differences are only in the third decimal.
6. F. Brogli and E. Heilbronner, Helv. Chim. Acta 54, 1423 (1971).

Figure Captions

Fig. 1. Relative iodine $3d_{5/2}$ binding energy vs. iodine $5p_{1/2}$ binding energy and least-squares straight line fit (slope = 1.22 ± 0.05) of all points except that for HI (▲).

Fig. 2. Diagram of the C-I bond length in relation to the average position of the 5p and 3d electrons. Note that r_{p-p}, the distance between the center of the C-I bond and the expected position of the 5p electron, is considerably longer than r_{p-d}.

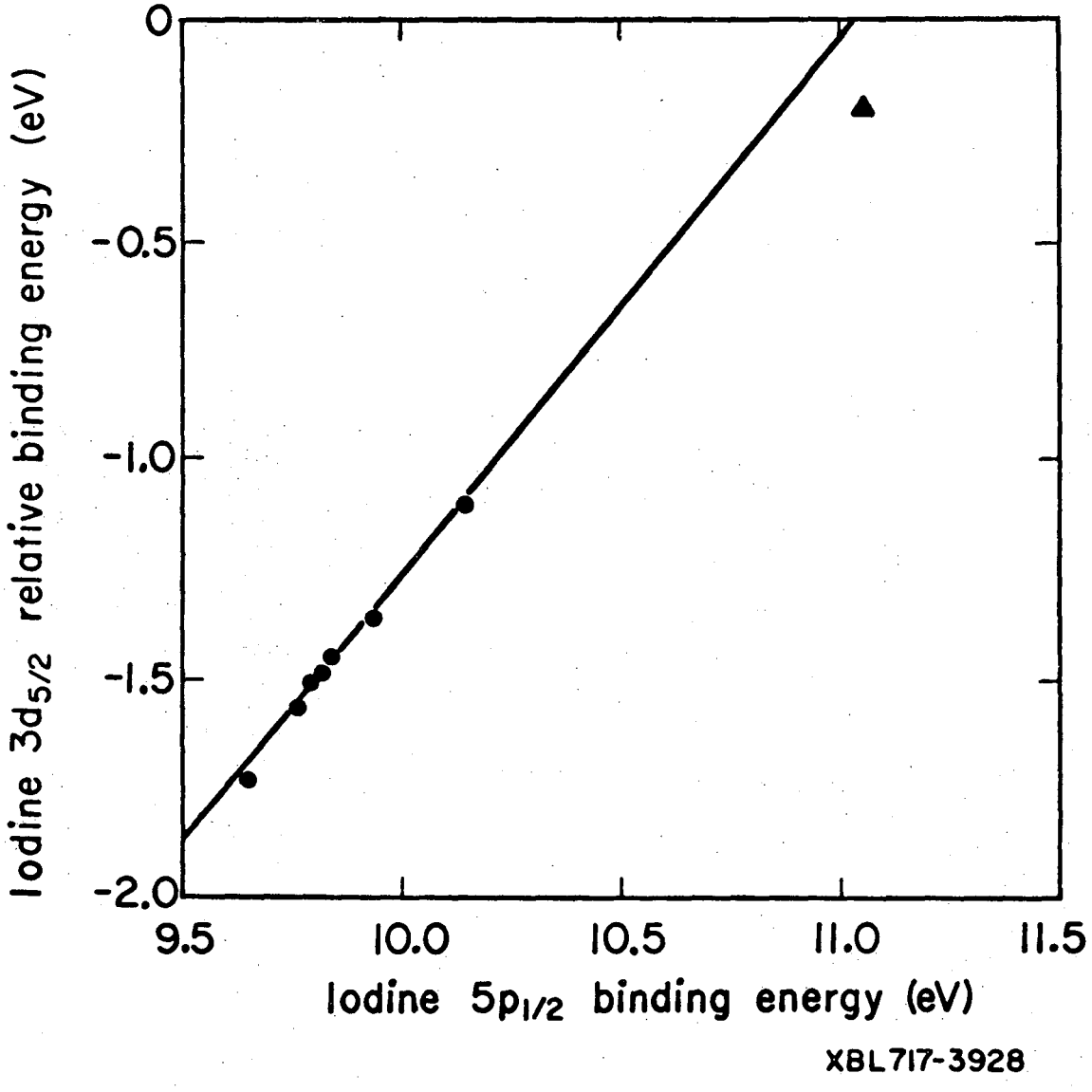
0
-0.5
-1.0
-1.5
-2.0
9.5
10.0
10.5
11.0
11.5
Iodine $3d_{5/2}$ relative binding energy (eV)
Iodine $5p_{1/2}$ binding energy (eV)
XBL717-3928

Fig. 1

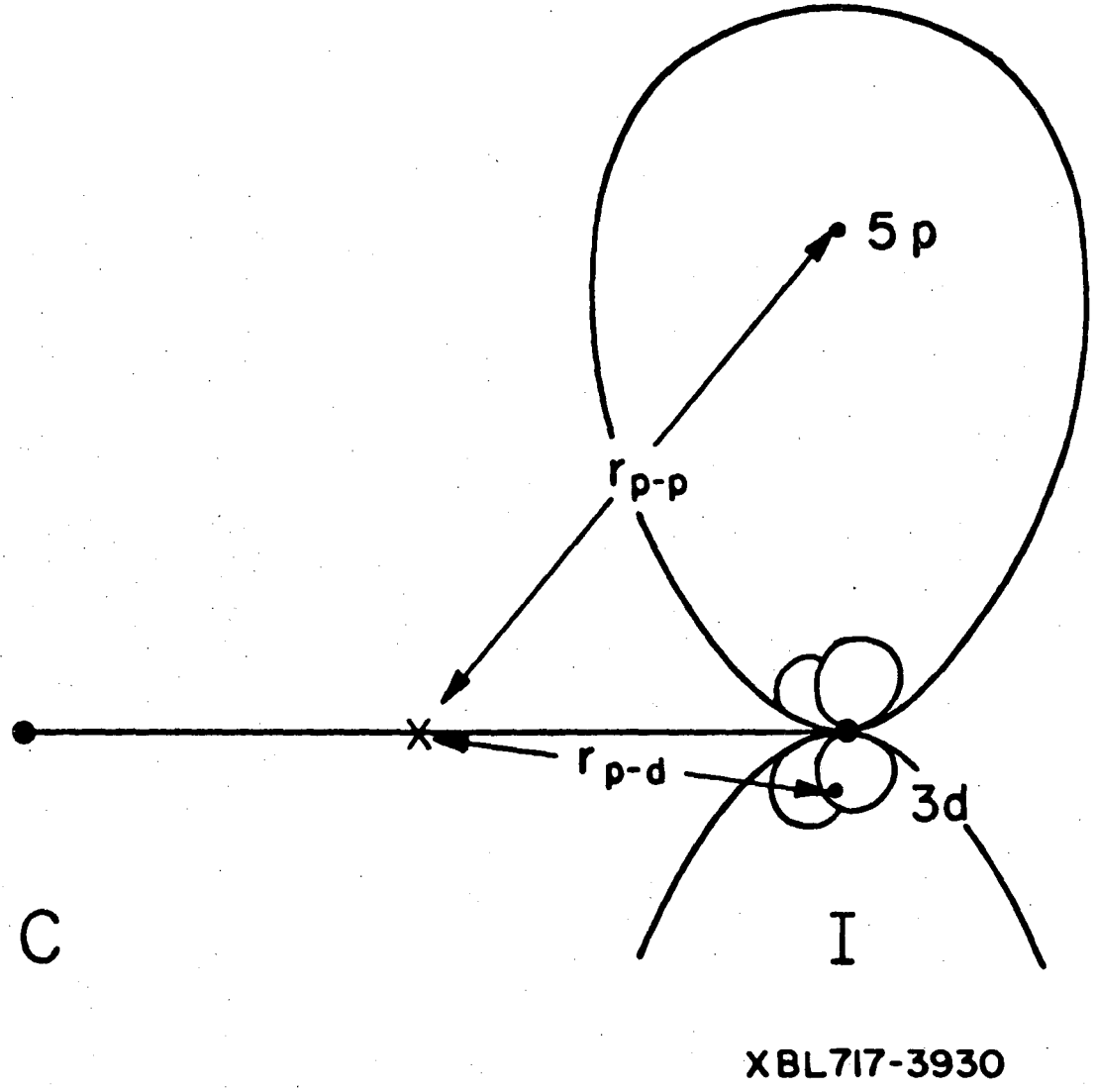

Fig. 2

II. STUDIES OF THE CORE BINDING ENERGY - PROTON AFFINITY CORRELATION IN MOLECULES

Abstract

Core-level binding-energy shifts were measured for O 1s levels in alcohols, ethers, acids, aldehydes, esters, and acetone; N 1s levels in ammonia and aliphatic amines, P 2p levels in phosphine and its methyl derivatives, and S 2p levels in H_2S and its methyl derivatives. A total of 46 compounds were studied. The core-level shifts correlated well with gas-phase proton affinities, thereby extending and supporting earlier results of Martin and Shirley, Davis and Rabalais, and Carroll, Smith, and Thomas. In the amines, for which the data are most precise, a good correlation was observed for all 16 molecules taken together. On a finer scale, each series of amines (primary, secondary, tertiary) showed a linear correlation, while ammonia and its methyl derivatives showed a linear correlation with different slopes. These two correlations are interpreted as responses of the system to long-range effects and to changes in the local bonds, respectively. Similar behavior was observed in the single-bonded oxygen compounds. Excellent linear correlations were observed in the compounds of the third period elements phosphorus and sulfur. Differences in the slopes were tentatively attributed to changes in nuclear position on protonation. Analysis of the oxygen data supports the conclusion of Carroll et al. that protonation of carboxyl groups occurs on the keto oxygen. These results suggest that core level shifts can be used to predict proton affinities.

Introduction

Chemists have devoted considerable effort to understanding the fundamental chemical concept of basicity. In a widely accepted early definition, Brønsted[1] described basicity as the tendency of a molecule B to accept a proton in the reaction

$$B + H^+ \rightarrow BH^+ \quad . \qquad -PA \qquad (1)$$

The enthalpy change of this reaction is -PA, where PA is the proton affinity of B. This concept of basicity was generalized further, and freed from reference to a specific acid (H^+) by Lewis, who defined a base as a molecule that tends to donate a valence electron "lone pair" in bonding with a Lewis acid; i.e., a molecule that can accept an electron pair.[2] Thus B in Eq. (1) is also a Lewis base because it contributed a lone pair in forming the B-H^+ bond.

Problems are encountered when attempting to relate these concepts to microscopic properties of isolated molecules. Measurements that yield basicity information are hard to make, and few are available. Gas-phase basicities can follow trends opposite to those observed in solution,[3] showing that the solution results may be dominated by solvation effects. It is of considerable importance to be able to separate the local molecular effects from those of solvation, because of the bearing of these two effects on the more general question of solution vs. gas-phase chemical reactivity. Recently Martin and Shirley,[4] and independently Davis and Rabalais,[5] have shown the relationship between trends in basicity and core-level binding energies.

They further showed that the trends in general resulted from the interplay of initial-state (inductive) effects and final-state (polarization) effects, with the latter dominating for the proton affinities and O 1s binding energies (E_B(O 1s)) of a series of aliphatic alcohols. This can be understood on the basis that the -OH group has essentially the same local charge distribution and electrostatic potential in different alcohols ROH. Introduction of a positive "test charge"--either by adding a proton to form ROH_2^+ or by removing an O 1s electron to form a positive 1s hole--is accompanied by a reaction energy that varies with R mainly through the variation of the R group's ability to stabilize the positive charge through polarization. The relation of the O 1s binding-energy trends with Lewis basicity is obvious, while its relation with Brønsted basicity is nearly quantitative for the few cores studied in references 4 and 5.

Carroll, Smith, and Thomas[6] added more single- and double-bonded oxygen compounds and some di- and triatomic molecules to the correlation between E_B(O 1s) and -PA, and they discussed the position of protonation for some cases. In this paper we report additional O 1s and N 1s core-level binding energies, and correlations with PA values in series of alcohols, ethers, acids, esters, aldehydes, acetone, and aliphatic amines. The correlation has been extended to the third row by measurements of core-level binding-energy shifts in phosphine and methyl-substituted phosphines, as well as the series H_2S, CH_3SH, $(CH_3)_2S$. Experimental procedures are described in the next section, and results are presented next. The results are discussed in the above order in the last section.

Experimental

All of the compounds were obtained commercially except for $P(CH_3)H_2$, which was made by the method given by Jolly.[7] The methyl-substituted phosphines were purified on a vacuum line, and their purities checked by vapor pressure measurements. Gaseous N_2, O_2, and PF_3, which were used as binding-energy standards, were run along with the appropriate compounds. The sulfur compounds were run with Ne as a standard. The spectra were taken on the 50-cm radius Berkeley magnetic spectrometer using Mg $K\alpha_{1,2}$ radiation. They were fitted to Gaussian peaks using a non-linear least-squares computer program. In the case of O_2, the two lines were fixed at an area ratio of 1 to 2 and a separation of 1.12 eV. For the acids and esters the peaks from the oxygens were constrained to have the same area.

Results

The binding energy shifts are shown in Table I along with the proton affinities for the various molecules studied. In some cases there was more than one literature value of the PA. In cases for which there was no clear reason to choose among various proton affinity values, preference was given to data in which an entire series was measured at the same laboratory. The worst disagreement is for acetone, in which the PA values are separated by 14 kcal while the stated errors are 2 kcal.[8,9]

The errors in the relative core binding energies are smaller than the PA errors in the oxygen compounds, amounting to 0.02 - 0.05 eV (0.5 - 1.2 kcal), being largest for molecules containing two oxygens where there is a problem of resolving two close peaks. This applies

to the acids, but is worse for the esters because of the smaller separation in the ester peaks. The relative errors in both PA and E_B for the amines are quite small.

Discussion

The relation of variations in proton affinity (PA), core-binding energy (E_B), and first (lone pair) ionization potential (IP) has been discussed previously.[4] Let us review this relationship briefly from two different points of view before discussing the data. First, the ionization potential corresponds to the reaction

$$B: \rightarrow B.^+ + e^- \qquad IP \quad , \tag{2}$$

where, as in Eq. (1), the reaction energy is written on the right. Combining Eqs. (1) and (2) with the binding energy of atomic hydrogen

$$H \rightarrow H^+ + e^- \qquad e^2/2a_o \quad , \tag{3}$$

we obtain

$$(B:H)^+ \rightarrow B.^+ + H \qquad HA \quad . \tag{4}$$

If the hydrogen affinity HA is constant as the base B is changed, it follows that $\Delta PA = -\Delta IP$. This condition is surely not satisfied in general, but we may expect it to be satisfied within a homologous series. For a series of alcohols ROH, for example, HA should be only weakly dependent on R. As a first approximation this weak R dependence of HA might be absorbed as a constant in the ΔPA vs. $-\Delta IP$ relation. Thus PA and -IP would vary together linearly, though not with unit slope. The core-level binding energy (E_B) can be incorporated ino

this linear variation if we note that E_B and IP should vary together (assuming that the lone pair is really an *atomic* pair), though not with unit slope.[10,11]

The second approach focuses on the similarity among the three processes, which for alcohols can be written

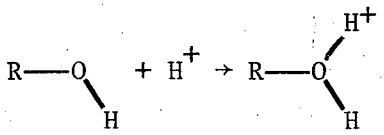

$$\text{R—O(H)} + H^+ \rightarrow \text{R—O(H)(H}^+\text{)} \qquad -PA \qquad (5a)$$

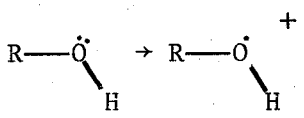

$$\text{R—}\ddot{\text{O}}\text{(H)} \rightarrow \text{R—O(H)}^+ \qquad IP \qquad (5b)$$

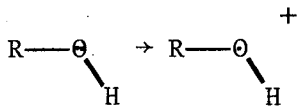

$$\text{R—}\Theta\text{(H)} \rightarrow \text{R—O(H)}^+ \qquad E_B(\text{O 1s}) \qquad (5c)$$

These equations were written to emphasize that in each case the ROH molecule is probed by a positive "test charge": the proton, the lone pair hole, and the 1s hole, at the OH bond distance, the O 2p radius, and the O 1s radius, respectively. While the absolute magnitudes of PA, IP, and E_B are very different, their *variation* in each case depends largely on the R group's ability to stabilize the added localized positive charge by polarization. Thus as R is varied -IP, PA, and E_B should vary together linearly, though not with exactly unit slope (the slope should be approximately unity[4,5]). Because the "lone pair" can have some molecular orbital character, it is the least reliable test probe. As the R group becomes larger the linear variation should become more reliable, provided that the local environment of the active

group is unchanged.

The data are discussed below in groupings that test various aspects of the correlation between E_B and PA.

Singly-Bonded Oxygen

Fig. 1 is a plot of E_B(O 1s) vs. PA for those molecules in which oxygen is only singly bonded. The line of unit slope through the water point falls typically 0.1 eV below the alcohol points and 0.35 eV below the ether points. The latter data sets are each well-fitted by lines of slope 0.95. It appears that substitution of an alkyl group for a hydrogen has a greater effect on E_B(O 1s) than on PA, although uncertainties in the PA shifts--which for those compounds are much less accurately known than the E_B(O 1s) shifts--leave a small residual doubt about this conclusion. The O 1s binding energies for OH groups in acids and esters are not included in Fig. 1 because the proton is believed to attach to the keto oxygen (see below). In fact these OH points would fall more than 1 eV below the lowest line in Fig. 1.

Doubly-Bonded Oxygen

The E_B(O 1s) values are plotted against proton affinities in Fig. 2, with the origin at the H_2O point. The acids and esters each showed two equally intense peaks in the O 1s spectra, with separations ranging from 1.28 eV to 1.79 eV for the various molecules. It is natural to expect that the lower binding-energy peak belongs to the doubly-bonded oxygen, on chemical grounds, because this oxygen is more negative. As pointed out by Carroll et al.,[6] theoretical estimates[12] of the O 1s binding energies in formic acid support this agreement. In order to determine which peak corresponds to the carbonyl oxygen without

invoking calculations or arguments about charge distribution, a spectrum of $CH_3O-\overset{O}{\overset{\|}{C}}-OCH_3$ (dimethyl carbonate) was obtained. This compound is very similar in structure to $CH_3(CH_2)-\overset{O}{\overset{\|}{C}}-OCH_3$ (methyl propionate) and gives a similar O 1s spectrum except that the high binding energy peak is twice the area of the other. This must therefore be the ether oxygen, and the low binding energy peak arises from the carbonyl oxygen. We are therefore confident that the O 1s peaks are correctly assigned in these compounds.

Although the E_B(O 1s) data do not by themselves give any indication of the protonation site in acids and esters, Carroll et al.[6] concluded from the E_B - PA correlation that protonation occurs at the keto oxygen, in disagreement with the assignment of Pesheck et al.[13] Our results agree with the assignment of Carroll et al. The "keto" oxygen correlation coincides with that of the aldehydes and ketones, while the "ether" oxygen correlation disagrees badly with the alcohol and ether values, as discussed above. Protonation apparently takes place at the keto oxygen.[14]

The range of E_B(O 1s) values in the doubly-bonded oxygen (Fig. 2) is actually somewhat larger than in the singly-bonded case (Fig. 1). This occurs in spite of the fact that in the keto linkage the "active" oxygen atom is always shielded by a carbon atom from shifts arising from changes of substituents. We believe that the larger range of E_B(1s) values--and of proton affinities--in the doubly-bonded oxygens arises because of an additive combination of inductive (initial-state) and polarization (final-state) effects. In the ether-linkage cases (Fig. 1), by contrast, inductive shifts were relatively small because

varying the alkyl groups did not change the oxygen very much.

The oxygen data can all be fitted reasonably well with the equation

$$PA = PA(H_2O) + 23.05[E_B(O\ 1s,H_2O) - E_B(O\ 1s,X)] - 7\ kcal \quad (6)$$

with proton affinities in kcal/mole and binding energies in eV. This equation should serve to predict proton affinities to ± 5 kcal or better. Of course it applies only to those oxygens on which proton attachment occurs.

Nitrogen 1s Binding Energies in Amines

Aliphatic amines comprise another series for which gas-phase PA values are available. Indeed Aue et al.[15] have reported an accurate set of PA values with small relative errors, although their values for ammonia and methyl amine were obtained by extrapolation of the PA-IP correlation. In Fig. 3 we have plotted E_B(N 1s) against the PA values. The E_B and PA scales are both relative, with ammonia taken as the reference compound. The absolute error in the PA of ammonia is shown in Fig. 3.

In discussing the systematics of the E_B(N 1s)-PA correlation, it is useful to divide the amines into primary, secondary, and tertiary groups, with methylamine, etc., comprising the first member of each group. We note first that a straight line of unit slope, Curve A, fits roughly through all the data. All but four of the sixteen compounds' points fall within 0.1 eV of Curve A, and the worst deviation is 0.15 eV. Thus the relation

$$\Delta E_B = -\Delta PA \quad (7)$$

is roughly confirmed.

The precision of the amine data permits a more detailed interpretation. Curve B, which is described by

$$\Delta E_B(\text{N 1s}) = -0.73\ \Delta PA \tag{8}$$

passes through ammonia and its three methyl derivatives. Its slope shows that PA varies faster than E_B(N 1s) when methyl is substituted for hydrogen. Within each amine series (primary, secondary, tertiary), however, the relation

$$\Delta E_B(\text{N 1s}) = -1.5\ \Delta PA \tag{9}$$

fits the data quite accurately. This means that within a series a change of the substituent affects E_B(N 1s) more than PA. The vertical IP within each series is also more sensitive to substituent change:[14]

$$\Delta IP = -1.4\ \Delta PA$$

The homolytic bond dissociation energy decreases upon substitution of larger alkyl groups. In fact we believe that all these observations can be interpreted in a self-consistent way that supports the earlier interpretations and yields additional insight into the proton addition reaction.

Two crucial points must be remembered:

1. The PA values are directly sensitive to details of local bonding at the nitrogen site, i.e., changes of angle, hybridization, etc. The vertical IP can be affected by hybridization and

hyperconjugation but not angle changes. The E_B(N 1s) parameter responds only to a change in the average potential, and may shift less.

2. If the local bonding at the nitrogen atom is kept constant, as in the series of primary amines for example, variations in the alkyl substituents will effect E_B, IP, and PA mainly through electron-electron shielding, either inductively (in the initial state) or through polarization in the final state. In either case the shift in E_B will exceed that in IP or PA.

The first point is consistent with the observation that in the group NH_3, methlyamine, dimethlyamine, trimethlyamine, the three quantities E_B, IP, and PA vary linearly with one another but with slopes very different from unity. The total ranges are ΔE_B = -0.7 eV, ΔIP = 2.3 eV, and ΔPA = -1.0 eV. The difference in sensitivities of IP on the one hand vs. E_B and PA on the other reflects the fact that the latter two quantities measure the molecule's response to a more localized test charge (a 1s hole or a proton), while the IP measures a much more complex property.

The second point can be interpreted more quantitatively. A distant perturbation (such as changing the length of an alkyl group) is felt locally at the nitrogen site through inductive or polarization effects. These are expressed as changes in the electron population in the valence shell of nitrogen in the initial and final states,

respectively. In either case the N 1s binding energy should vary as the two-electron Coulomb integral $F^0(1s,2p)$ times Δn, the change in valence shell population, while for the IP this integral is replaced by $F^0(2p,2p)$. This leads to larger shifts for inner shells, a well-known effect that has been discussed elsewhere.[10,11] We note for a proton at the mean radius of the 2p shell in nitrogen the Coulombic interaction with N 2p electrons would be of a similar magnitude but opposite sign compared to a 2p electron-electron interaction. Since, however, the proton is $\sim$0.3 Å farther from the nucleus than the expectation value for the radius of a 2p electron, the shielding effect should be smaller. We therefore would predict

$$\frac{\Delta E_B(\text{N 1s})}{\Delta \text{IP}} \cong \frac{F^0(1s,2p)}{F^0(2p,2p)} = 1.45 \quad ,$$

$$\left|\frac{\Delta \text{IP}}{\Delta \text{PA}}\right| > 1 \quad ,$$

for the slope within a series of primary, etc., amines. The numerical ratio 1.45 was obtained by using Mann's integrals.[16] This is the ordering we see.

Shifts in Sulfur and Phosphorus

The E_B - PA comparison was extended to third-row elements by studying H_2S, phosphine, and their methyl derivatives. Sulfur and phosphorus differ from oxygen and nitrogen in having larger covalent radii, low-lying d orbitals, and lower electronegativity. Thus it was not clear what to expect. Only seven molecules were studied in this first attempt to extend the E_B - PA correlation to the third row,

so only tentative conclusions can be drawn as yet. Thus far a surprisingly good correlation appears to exist.

Fig. 4 shows a linear E_B(P 2p) - PA correlation in the phosphorus compounds, but the slope is significantly less than one. This is interesting because the first IP follows the PA much more closely[17] (just the opposite from the amines). In other words, the homolytic bond dissociation is about constant. Nuclear rearrangement, or relaxation, in the protonated final state is important in the phosphines. This nuclear relaxation takes place upon protonation and with removal of a lone pair electron (for the *adiabatic* IP) but not in the case of core ionization. It is possible to estimate the degree of angular rearrangment of the phosphines from the bond angles in the corresponding silanes, which are isoelectronic in the valence shells and have equal core charge. The H-P-H angle in phosphine is 93.3°, and the protonated ion is tetrahedral (109.5°). The corresponding angle change in trimethylphosphine is 98.9° to 110.2°. CNDO/2 calculations indicate that in the ground state the lone pair orbital is mainly s-like, whereas in the protonated state the P-H bond is more nearly sp^3 in character. The steric strain moderation on substituting a less replusive hydrogen for a lone pair is expected to be greater in the case of the methylated phosphines than in phosphine itself where the hydrogens are already over 2 Å apart in the initial state. Similar angle opening is expected upon ionization of one of the lone pair electrons because a single electron is also less repulsive than a lone pair. Core ionization, however, should not cause significant angular relaxation. This might account for the poorer agreement between $-\Delta PA$ and ΔE_B than between

$-\Delta PA$ and ΔIP. Of course there may be another reason for the observed behavior. Perhaps, for example, the fact that the ΔE_B-ΔPA correlation shows a low slope in the methyl derivatives of nitrogen and phosphorus (-0.7 and -0.6, respectively) is a clue that the same mechanism is operative in both cases.

In considering the sulfur compounds we first note that there are only three points and that the PA measurements were done by two different groups. It may, therefore, be fortuitous that $-\Delta PA = \Delta E_B$ to within experimental error (Table I). Unfortunately for geometry change arguments for the type used above for the phosphines, we do not have the geometries for CH_3PH_2 or $(CH_3)_2PH$ which are isoelectronic with $CH_3SH_2^+$ and $(CH_3)_2SH^+$. If we assume, however, that the angles of the above phosphorus compounds are intermediate between those of PH_3 and $P(CH_3)_3$, the angles between the ligand bonds in CH_3SH and $(CH_3)_2S$ would *decrease* upon protonation. Comparison of SH_2 and PH_3 indicates that the H-S-H angle increases by only 1° upon protonation. While these arguments are not quantitative, it appears that relief of steric strain in the final protonated state is less important for the sulfur series.

Conclusions

The binding energy-proton affinity correlation has been extended by this work to forty-six molecules, including molecules containing the third-row elements phosphorus and sulfur. The following conclusions were drawn:

1. The correlation holds up surprisingly well in the main, in both second- and third-row elements.

2. Extension to ethers (from H_2O and alcohols) and to larger alkyl amines shows that two correlations exist. All primary amines fall on one line, for example, while secondary amines are offset. This reflects the relative sensitivities of E_B and PA to long-range inductive effects versus changes in local bonding. It may prove valuable in understanding variations in proton affinity.
3. Further evidence was obtained that protonation of carboxyl groups takes place at the keto oxygen.
4. The small slope of the correlation in phosphine derivatives and the unit slope in H_2S derivatives may be a consequence of nuclear relaxation, because the bond angles appear to change more in the former case.

The main conclusion to be drawn is that these additional results tie core-level binding-energy shifts firmly to a chemical property, the proton affinity. The proton and the core electron can be regarded as two "test charges" that probe both the static (initial-state) and dynamic (final-state) properties of a functional group. Used in a complementary way these two probes may yield insight into the electron dynamics of chemical reactions.

References

1. J. N. Brønsted, Rec. Trav. Chim. 42, 718 (1923).
2. G. N. Lewis, "Valence", Dover Publications, New York, N.Y. (1966), p. 142.
3. J. I. Brauman and L. K. Blatt, J. Amer. Chem. Soc. 90, 6562 (1968); J. I. Brauman, J. M. Riveros, and L. K. Blair, ibid, 93, 3914 (1971); and references cited therein.
4. R. L. Martin and D. A. Shirley, J. Amer. Chem. Soc. 96, 5299 (1974).
5. D. W. Davis and W. Rabalais, J. Amer. Chem. Soc. 96, 5305 (1974).
6. T. X. Carroll, S. R. Smith, and T. D. Thomas, J. Amer. Chem. Soc. 97, 659 (1975).
7. W. L. Jolly, Inorganic Syntheses, 11, 124 (1968).
8. J. Long and B. Munson, J. Amer. Chem. Soc. 95, 2427 (1973); L. Hellner and L. W. Sieck, J. Res. Nat. Bur. Stand., Section A, 75, 487 (1971).
9. M. A. Haney and J. L. Franklin, J. Phys. Chem. 73, 4328 (1969).
10. D. A. Shirley, "ESCA", Advan. Chem. Phys. 23, 85 (1973).
11. J. A. Hashmall, B. E. Mills, D. A. Shirley, and A. Streitwieser, Jr., J. Amer. Chem. Soc. 94, 4445 (1972).
12. D. W. Davis and D. A. Shirley, J. Electr. Spectros. Relat. Phenomena 3, 173 (1974).
13. C. V. Pesheck and S. E. Buttrill, Jr., J. Amer. Chem. Soc. 96, 6027 (1974).
14. D. H. Aue, H. M. Webb, and M. T. Bowers, J. Amer. Chem. Soc. 98, 311 (1976).

15. D. H. Aue, H. M. Webb, M. T. Bowers, J. Amer. Chem. Soc. 94, 4726 (1972).

16. J. B. Mann, "Atomic Structure Calculations I. Hartree-Fock Energy Results for the Elements Hydrogen to Lawrencium", LA-3690, TID 4500.

17. R. H. Staley and J. L. Beauchamp, J. Amer. Chem. Soc. 96, 6252 (1974).

TABLE 1. Binding energy shift from reference molecule, proton affinity and shifts relative to the basic hydride.

Molecule	$-E_B$ Shift		PA Used	Other PA measurements	$-\Delta E_B$	ΔPA
Water	3.43(2)		165(3)[a]	165(3)[b], 164(4)[c]	0.00	0(3)
Methanol	4.22(2)		180(3)[d]	182(3)[b]	0.79	15(3)
Ethanol	4.53(2)		187(2)[a]	186[d]	1.10	22(2)
Propanol	4.60(2)		189(2)[a]		1.17	24(2)
i-Propanol	4.75(2)		193(5)[a]	193(5)[e], 195[f]	1.32	28(5)
t-Butanol	4.96(2)		198(3)[a]	206[f]	1.53	33(3)
Dimethyl ether	4.74(2)		187(1)[d]	190(5)[a], 186[d], 186[e]	1.31	22(1)
Diethyl ether	5.24(2)		199[b]	205(3)[a]	1.81	34
Formaldehyde	3.77(2)		168(1)[g]	166[d], 165(3)[c]	0.34	3(1)
Acetaldehyde	4.71(2)		185(2)[g]	183(2)[e], 183[d]	1.28	20(2)
Propionaldehyde	4.85(2)		187(2)[g]	187[d]	1.42	22(2)
Acetone	5.37(2)		202(2)[a]	188(2)[b], 196(2)[h], 202[i]	1.94	37(2)
Formic acid	2.65(3)	4.35(3)	175(5)[a]	179(3)[b], 166[j]	0.92	10(5)
Acetic acid	3.20(3)	4.99(3)	188(3)[a]	184(3)[j]	1.56	23(3)
Propionic acid	3.31(3)	5.07(3)	~190[a]	185(3)[j]	1.64	~25
Trifluoroacetic acid	2.00(3)	3.75(3)	167(3)[a]		0.32	2(3)
Methyl formate	3.46(5)	4.86(5)	188(3)[a]		1.43	23(3)
Ethyl formate	3.72(5)	5.01(5)	198(3)[a]		1.58	33(3)
Propyl formate	3.80(5)	5.08(5)	198(3)[a]		1.65	33(3)
Methyl acetate	3.86(5)	5.39(5)	202(2)[a]		1.96	37(2)
Ethyl acetate	4.07(5)	5.49(5)	205(3)[a]		2.06	40(3)
Propyl acetate	4.13(5)	5.55(5)	207(3)[a]		2.12	42(3)
Methyl propionate	4.03(5)	5.58(5)	205(3)[a]		2.15	40(3)
Ammonia	4.41(2)		207(3)[k,l]		0.00	0(3)
Methylamine	4.76(2)		218.4[l]	211(3)[b], 216.3(6)[m]	0.35	11.4
Ethylamine	4.95(2)		221.4[l]	218.8(6)[m]	0.54	14.4
n-Propylamine	5.03(2)		222.8[l]		0.62	15.8
n-Butylamine	5.05(2)		223.3[l]		0.64	16.3
i-Propylamine	5.11(2)		223.7[l]	221.2(6)[m]	0.70	16.7
sec-Butylamine	5.19(2)		224.8[l]		0.78	17.8
t-Butylamine	5.24(2)		225.7[l]	223.3(6)[m]	0.83	18.7
Dimethylamine	5.00(2)		224.8[l]	222.4(6)[m]	0.59	17.8
Diethylamine	5.36(2)		229.4[l]		0.95	22.4
Di-*n*-propylamine	5.46(2)		231.4[l]		1.05	24.4
Di-*n*-butylamine	5.50(2)		232.5[l]		1.09	25.5
Di-*i*-propylamine	5.62(2)		233.2[l]		1.21	26.2

continued . . . .

TABLE 1 (continued)

Molecule	$-E_B$ Shift	PA Used	Other PA measurements	$-\Delta E_B$	ΔPA
Trimethylamine	5.11(2)	228.6[l]	226.6(6)[m]	0.70	21.6
Triethylamine	5.59(2)	235.5[l]		1.18	28.5
Tri-*n*-propylamine	5.71(2)	237.7[l]		1.30	30.7
Phosphine	4.70(2)	187.9[n]		0.00	0.0
Methylphosphine	5.23(2)	206.9[n]		0.53	19.0
Dimethylphosphine	5.55(2)	218.9[n]		0.85	31.0
Trimethylphosphine	5.78(2)	228.0[n]		1.08	40.1
Hydrogen sulfide	0.00	170(3)[k]		0.00	0.0
Methanethiol	0.69(3)	186[d]		0.69(3)	16
Dimethyl sulfide	1.18(3)	197[d]		1.18(3)	27

[a] J. Long and B. Munson, J. Amer. Chem. Soc. 95, 2427 (1973).

[b] M. A. Haney and J. L. Franklin, J. Phys. Chem. 73, 4328 (1969).

[c] J. L. Beauchamp and S. E. Buttrill, Jr., J. Chem. Phys. 48, 1783 (1968).

[d] J. L. Beauchamp, Annu. Rev. Phys. Chem. 22, 527 (1971).

[e] J. L. Beauchamp and R. C. Dunbar, J. Amer. Chem. Soc. 92, 1477 (1970).

[f] J. L. Beauchamp and M. C. Caserio, ibid, 94, 2638 (1972).

[g] K. M. A. Refaey and W. A. Chupka, J. Chem. Phys. 48, 5205 (1968).

[h] V. K. Potapov and V. V. Sorokin, High Energy Chem. (USSR) 4, 508 (1970).

[i] L. Hellner and L. W. Sieck, J. Res. Nat. Bur. Stnd., Section A, 75, 487 (1971).

[j] J. Long, Ph.D. Thesis, University of Delaware (May 1972).

[k] M. A. Haney and J. L. Franklin, J. Chem. Phys., 50, 2028 (1969).

[l] D. H. Aue, H. M. Webb, and M. T. Bowers, J. Amer. Chem. Soc., 98, 311 (1976).

[m] W. G. Henderson, M. Taagepera, D. Holtz, R. T. McIver, Jr., J. L. Beauchamp and R. W. Taft, J. Amer. Chem. Soc. 94, 4728 (1972).

[n] R. H. Staley and J. L. Beauchamp, ibid, 96, 6252 (1974).

Figure Captions

Fig. 1. Oxygen 1s binding energies versus proton affinities for single-bonded oxygens. Water is taken as the reference compound. Alcohols are denoted by circles and ethers by squares. The top two lines have slopes of 0.95, and the lowest line has unit slope. Errors in PA are shown: errors in E_B are smaller than symbols.

Fig. 2. Oxygen 1s binding energies versus proton affinities for double-bonded oxygen in acids (circles), esters (squares), aldehydes (diamonds), and acetone (triangle). The two lines of unit slope are offset by 0.4 eV. They pass through the data and the water reference point, respectively.

Fig. 3. Nitrogen 1s binding energies versus proton affinities for a series of aliphatic amines (Table I), using ammonia (triangle) as a reference. Primary amines are shown as open circles, secondary amines as filled circles, and tertiary amines as squares. Line A has slope unity and is drawn through all the data. Line B connects the ammonia, methylamine, dimethlyamine, and trimethlyamine points. The other lines show the linear variation within each series.

Fig. 4. Phosphorus 2p binding energies plotted against proton affinity for phosphine and its methyl derivatives. The variation is linear, with a slope of 0.6.

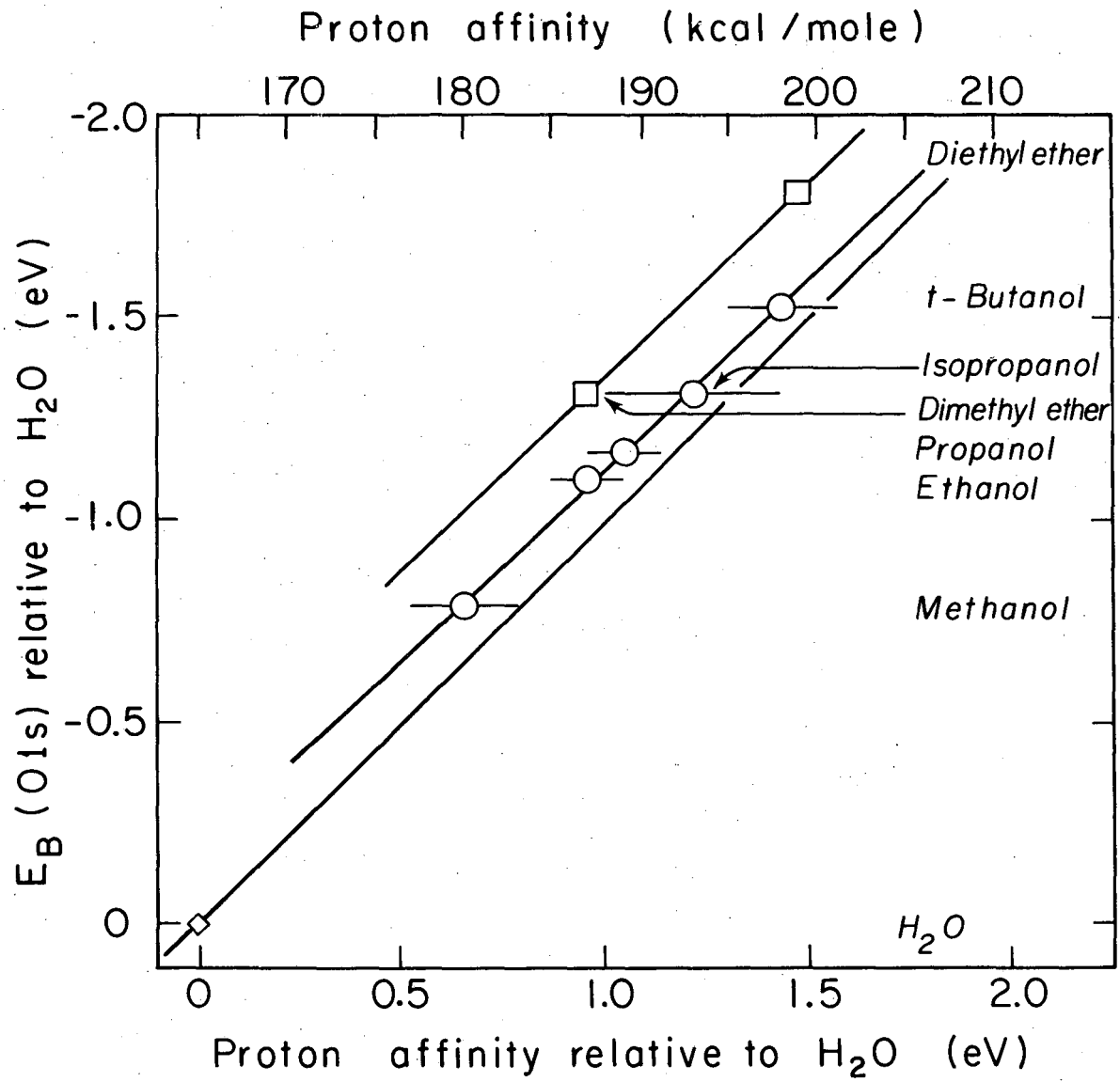

XBL756-3296

Fig. 1

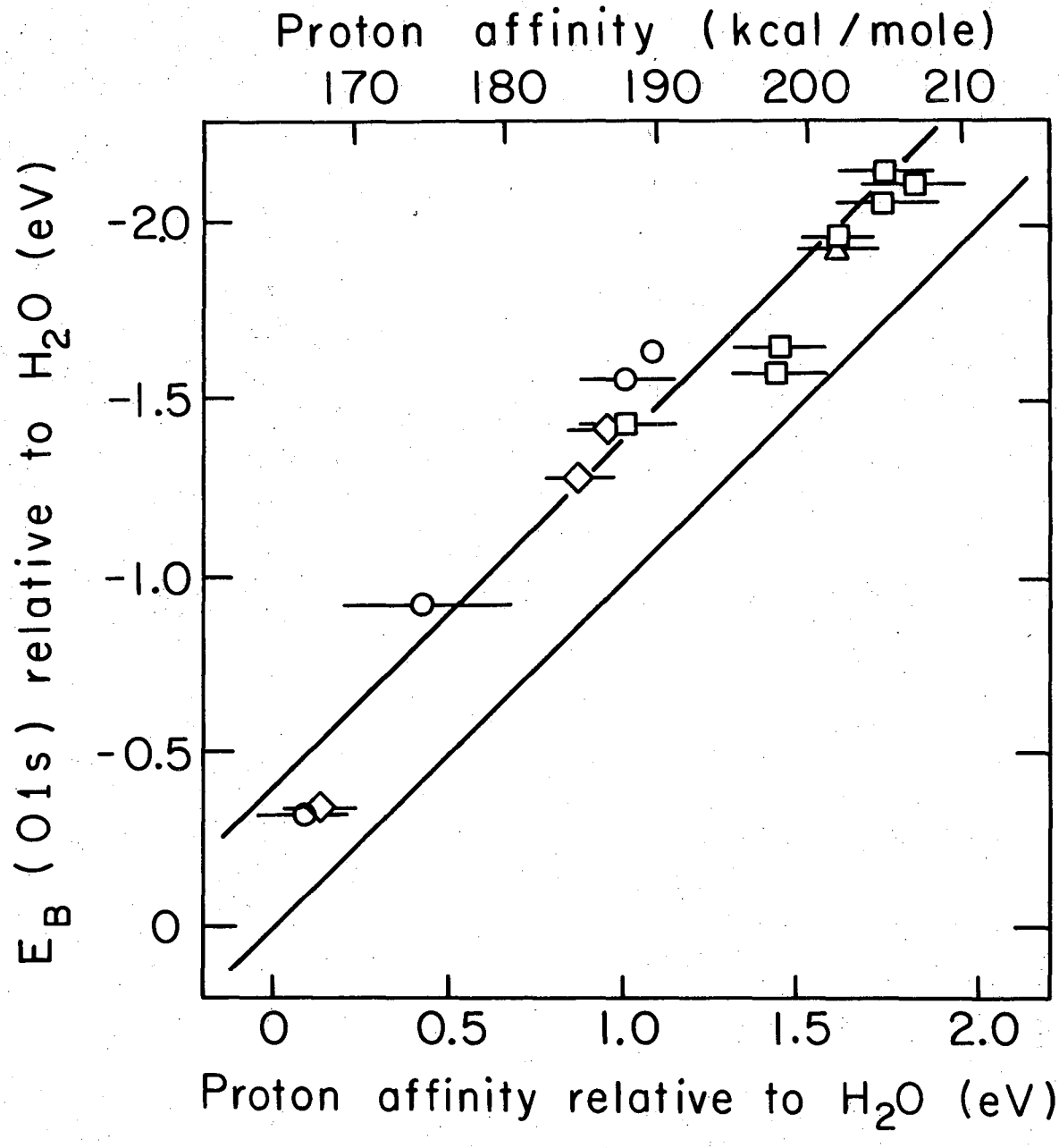

XBL756 - 3298

Fig. 2

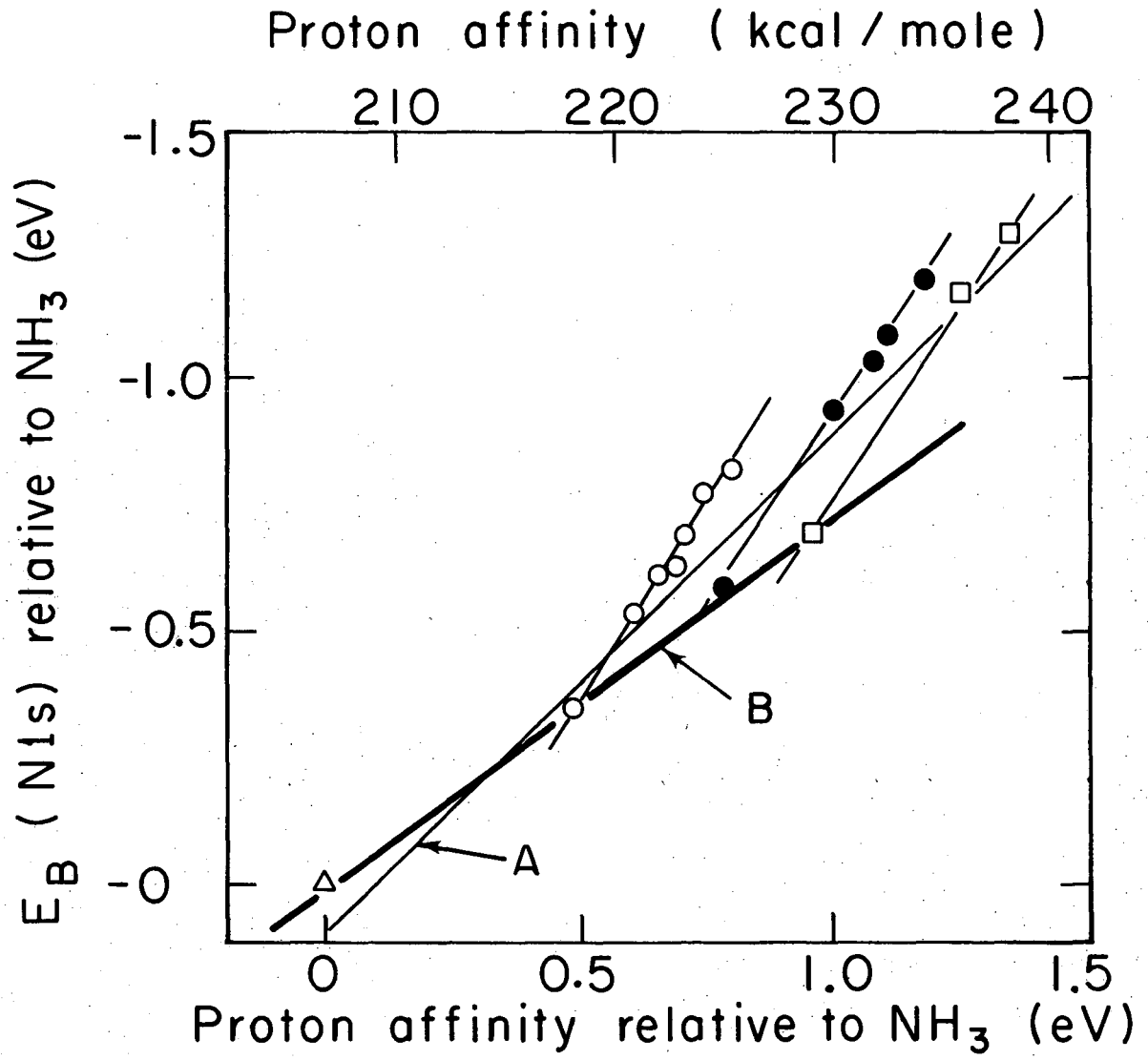

XBL756-3297

Fig. 3

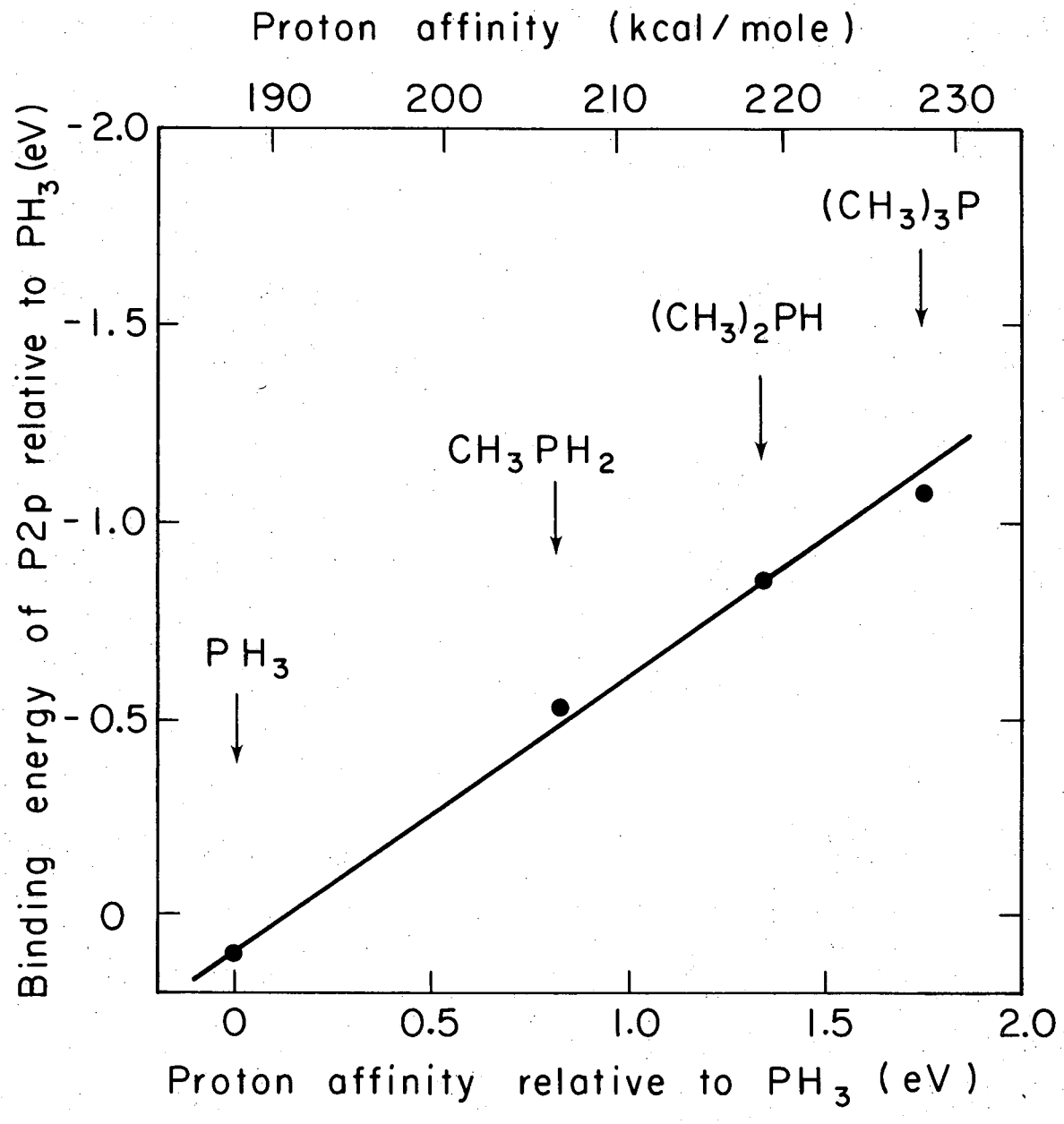

XBL756-3295

Fig. 4

III. X-RAY PHOTOEMISSION MOLECULAR ORBITALS OF HYDROGEN FLUORIDE AND THE FLUORINATED METHANES

Abstract

The x-ray photoemission molecular orbital spectra of gaseous hydrogen fluoride and the fluorinated methanes (CH_nF_{4-n}, $0 \leq n \leq 4$) are reported. Ab initio, Koopmans' theorem energies and a three-parameter relaxation model were used to fit the experimental binding energies. Excellent agreement was obtained. Relative intensities of molecular orbitals were computed using the model of Gelius with both CNDO/2 and ab initio atomic populations. In the case of ab initio results, net populations were found to be superior to gross populations in reproducing the experimental intensities. In most cases the theory predicted intensities quite well. Some trends exhibited by the fluoromethane series are noted.

Introduction

The development of molecular photoelectron spectroscopy[1,2] has made it possible to establish the binding energies of individual molecular orbitals (MO's). Detailed analyses of spectra can yield further information concerning the electronic structure of the molecule. For example, Gelius[3] has proposed that x-ray photoemission (XPS) cross sections of MO's should be given approximately by a sum of atomic orbital (AO) cross sections, weighted according to the contribution of each AO to the MO in question. Thus, if ψ_i represents an MO that can be expressed as a linear combination of atomic orbitals ϕ,

$$\psi_i = \sum_j C_{ij} \phi_j \quad , \tag{1}$$

the x-ray photoemission cross section σ_j is given approximately by

$$\sigma_i(\text{MO}) \cong \sum_j P_{ij} \sigma_j(\text{AO}) \quad . \tag{2}$$

Here P_{ij} gives the electron population in AO ϕ_j given an electron in MO ψ_i. The essential physics behind the validity and usefulness of Eg. (2) arises from the fact that the dipole matrix element for the transition can be reduced to an overlap integral between an MO and the photoelectron final state. (For example, the latter can be represented by a plane wave orthogonalized to the core.) For x-ray energies, this overlap integral has large contributions only near the nuclei, where the strong nuclear potential is dominant and the curvature of the MO radial wave function matches that of the outgoing electron. In XPS the photoelectron's de Broglie wavelength is approximately 0.35 Å (using Mg Kα x-rays) or 0.32 Å (with Aℓ Kα x-rays) for initial states

in the entire MO region. Of course, this argument and Eq. (2) would not apply to ultraviolet photoemission spectroscopy (UPS) because the longer wavelength of the photoelectron makes the photoelectric cross section sensitive to the curvature of the orbitals in the bonding regions, and because the percentage energy variation over the MO region is large.

A second assumption must be made when the electron populations P_{ij} are expressed in terms of the expansion coefficients C_{ij}. The quantities P_{ij} have no unique rigorous meaning, and this step is somewhat arbitrary. Even when ab initio MO calculations are employed, one must decide between "net" or "gross" populations,[4] or among other schemes. Further possibilities are introduced by the use of more approximate MO theories.

Irrespective of the details of the particular analysis that is adopted, the Gelius model should have considerable diagnostic value even if Eq. (2) is not completely rigorous. Ideally, a given set of calculated XPS atomic cross-sections $\{\sigma(AO)\}$ and a set of measured XPS MO cross-sections $\{\sigma(MO)\}$, would indicate whether a given set of populations $\{P_{ij}\}$ are consistent with the experiment.

The work reported below was undertaken to acquire some insight into the usefulness of the Gelius model. The fluorinated methanes were chosen as the model system because they have already been studied by UPS and are large enough to be challenging but small enough to be tractable, both spectroscopically and theoretically. The XPS experiments are described in the next section. Then comparison of orbital binding energies with earlier work and with theory are made.

Intensities and spectroscopic assignments for individual molecular species are discussed. Finally, trends through the whole series are treated.

Experimental

Samples were obtained from Matheson Gas Co. and studied in the gas phase with the Berkeley Iron-Free Spectrometer.[5] They were irradiated with Mg $K\alpha_{1,2}$ (1.2536 keV) or Aℓ $K\alpha_{1,2}$ (1.4866 keV) x-rays using sample pressures of 50 to 100μ. Photoelectrons emitted perpendicular to the x-ray beam were focused and counted at kinetic energy increments of ∿0.33 eV and in some cases (in the region up to 30 eV binding energies) at increments of ∿0.16 eV. Binding energies were calibrated in one of two ways. In some cases neon was run together with the gas under study and the neon 2s (48.42 eV)[2,6] or the neon 2p (21.59 eV)[2] level was scanned with part of the MO region of the gas in question. In other cases, one of the core levels (F 1s or C 1s) was scanned alternately with the MO region. Then, in a separate run, that core level was referenced to one of the neon valence levels. The two methods gave results in good agreement.

Lorentzian functions were non-linear least-squares fitted to the experimental spectra and used to determine the peak positions and areas. Provision was automatically made in the fitting program for the $K\alpha_3$ and $K\alpha_4$ x-ray satellites at kinetic energies 8.412 eV and 10.142 eV higher than the main $K\alpha_{1,2}$ exciting line. In general, it was found that Lorentzians reproduced the experimental peaks shapes better than Gaussians, but this does not imply that lifetime broadening is a dominant contributor to the linewidth, because the spectrometer

response function is made up of several contributing factors of similar magnitude, and the composite function is rather well approximated by a Lorentzian.

Orbital Binding Energies

The XPS molecular orbital spectra of HF and the five gases $CH_{4-n}F_n$ ($0 \leqslant n \leqslant 4$) are shown in Fig. 1. Except for the CH_4 spectrum, which was taken with Aℓ $K\alpha_{1,2}$ radiation (in order to reduce the interference of the $K\alpha_3$ and $K\alpha_4$ satellites), all measurements were made using the Mg $K\alpha_{1,2}$ line. The measured binding energies, $E_B(MO)$, are given in Table I and compared to the vertical binding energies measured by UPS.[7,8] Brundle, Robin, and Basch[8] reported a systematic study of the fluoromethane series using He I and He II radiation. They also tabulated some vertical E_B values obtained by earlier workers. Since there is good agreement on the experimental values of E_B (as distinguished from the interpretations), in the cases for which duplicate values are available from earlier studies, we shall simply refer to the tabulation of Brundle et al.,[8] rather than intercomparing the available UPS results. Our interest here is in comparing our XPS $E_B(MO)$ values with the UPS vertical $E_B(MO)$ results. The agreement between the two sets of values is generally excellent, in most cases within 0.1 or 0.2 eV.

Comparison of experimental $E_B(MO)$ values with theory is less straightforward, because self-consistent field calculations of the molecular ground states yield only the orbital energies, $\varepsilon(MO)$, rather than actual binding energies, $E_B(MO)$, of the molecular orbitals. It is in principle possible to calculate $E_B(MO)$ directly by the

Δ(self-consistent-field) method, in which one calculates the total energy of each final (hole) state and subtracts the total energy of the ground state. This approach is not generally applicable, however, because of expense and convergence problems, and we shall follow the usual practice in interpreting photoemission spectra, of employing SCF calculations only in the molecular ground state.

Even within this restricted framework there is some freedom of choice, as the level of sophistication of the SCF calculation can vary considerably. We have chosen to compare the experimental energies with theoretical orbital energies obtained by Snyder and Basch[9] from ab initio POLYATOM calculations using Gaussian-type orbitals. We have also made CNDO/2 calculations for comparison. Orbital energies from both calculations are listed in Table I.

For each MO, comparison of the figures in Table I establishes the order

$$E_B(\mathrm{MO}) < -\varepsilon(\mathrm{MO})_{\underline{ab\ initio}} < -\varepsilon(\mathrm{MO})_{\mathrm{CNDO/2}} \quad .$$

The CNDO/2 approach is known to give unreliable energies, and little further discussion seems warranted here. We note that reduction of the $-\varepsilon_{\mathrm{CNDO/2}}$ values by 20% will give energies that agree on the whole fairly well. The level ordering is usually correct, but there are several errors, and energy discrepancies of 2 eV between 0.80 ($-\varepsilon_{\mathrm{CNDO/2}}$) and E_B are present in some cases. It would be fruitless to attempt to rationalize the remaining discrepancies because the nature of the CNDO/2 approach makes it difficult to distinguish computational approximations from real physical effects. Considerable improvement

could be obtained using the multiple-scattering Xα method.[10] This type of calculation employs a local exchange potential (proportional to the cube root of the electronic density multiplied by an exchange scaling parameter α) to accurately approximate the solutions of the Hartree-Fock equations. The resulting Xα one-electron equations are solved using the multiple-scattering computational technique.[11]

In comparing $E_B(MO)$ and $-\varepsilon(MO)_{\underline{ab\ initio}}$ the accuracy of the latter is high enough that most of the difference can realistically be attributed to physical effects. The binding energy and orbital energy are related by

$$E_B(MO) = -\varepsilon(MO) - E_R(MO) + \Delta E(MO)_{corr} + \Delta E(MO)_{rel} \quad . \qquad (3)$$

Here $E_R(MO)$ is the relaxation energy of the final state with a hole in the molecular orbital under study, and $\Delta E(MO)_{corr}$ and $\Delta E(MO)_{rel}$, which may have either sign, are the excess correlation and relativistic energies in the final state over those in the initial state. We shall neglect these last two terms for lack of a good approximate method of dealing with them, noting that they are usually relatively small (i.e., 1 eV or less) in the cases studied here.

The E_R term is often larger and always positive. It arises because the wave functions of the passive electrons relax during photoemission from an N-electron system, lowering the energy of the hole state. This phenomenon is usually discussed in connection with Koopmans' Theorem,[12] which states the approximate equility $E_B(MO) \cong -\varepsilon(MO)$. Since E_R tends to increase with E_B, it has become

customary to correct for E_R empirically by reducing $-\varepsilon$ by some fixed percentage. Thus, Brundle et al.[8] found that the approximate relation E_B (theo) $\cong 0.92\ (-\varepsilon)$ gave a rather good estimate of binding energies in the fluorinated methanes.

With the increased understanding of atomic and extra-atomic relaxation energies accompanying photoemission that has emerged recently, it appears possible to improve our estimates of E_B(MO) from ε(MO). The fluorinated-methane molecular-orbital E_B values determined by XPS require a more sophisticated approach and also provide insight as to how it should be developed. The spectrum of each fluorinated species in Fig. 1 includes one or two orbitals with E_B near 40 eV, considerably more tightly bound than the rest. These are the orbitals made up primarily of fluorine 2s functions in the atomic-orbital expansion. Although their eigenstates are irreducible representations of the molecular symmetry groups (hence the splitting into $3a_1$ and $2b_1$ in CH_2F_2, etc.), these orbitals are also partially core-like in their behavior. They appear to have E_R values of $\sim$6 eV, close to the E_R value of 4.9 eV[13] for the 2s level in F^-.

We note also that the $2a_1$ level in HF, which is mostly F 2s in character, shows E_R = 4.2 eV. These "F 2s-like" levels would require a correction of 12-13% to bring $-\varepsilon$ in line with E_B in the fluorinated methanes, rather than the 8% used by Brundle et al.[8] for the less tightly-bound orbitals. As a first step in determining whether it might be useful to take AO character into account in correcting $-\varepsilon$ values for relaxation, we have listed the quantity

$$\Delta\varepsilon_{ai} \equiv -\varepsilon_{\underline{ab\ initio}} - E_B(\text{XPS})$$

for each orbital, in Table I. Inspection of these $\Delta\varepsilon_{ai}$ values, and comparison with the ε and E_B columns readily reveals several facts:

1. For each molecule the $\Delta\varepsilon$ values for the F 2s-like MO's are much larger than those for the other MO's and $\Delta\varepsilon/\varepsilon$ is somewhat larger.
2. Within each group of non-F 2s-like orbitals the correlation between $\Delta\varepsilon$ and ε is not very strong.
3. For both types of orbital, $\overline{\Delta\varepsilon}$ increases with the total number of valence electrons in the molecule, where $\overline{\Delta\varepsilon}$ is defined as the average $\Delta\varepsilon$ for a given type of orbital in each molecule.

Parts of both 1 and 3 could be "explained" by assuming $\Delta\varepsilon/\varepsilon$ constant throughout, but this approach does not satisfy all of 1 and 3, nor does it help with 2. To provide estimates of E_B from ε that are both more accurate and theoretically sounder, we propose below a model for E_R that is based on recent studies[14-16] of the role of relaxation energies in core-level binding energies.

Relaxation energies can be somewhat arbitrarily separated into atomic and extra-atomic contributions,

$$E_R = E_R^{\,a} + E_R^{\,ea} \quad . \tag{4}$$

For core levels the atomic term E_R^a is relatively well-defined, as is the above separation. For molecular orbitals ψ_i given by Eq. (1) a first approximation to E_R^a (MO,i) would be given by

$$E_R^a \text{ (MO,i)} = \sum_j |C_{ij}|^2 \, E_R^a \text{ (AO,j)} \quad , \tag{5}$$

where E_R^a (AO,j) is the relaxation energy of atomic ortibal ϕ_j. The E_R^{ea} term is more difficult to estimate, but it would be expected to increase with molecular size, in analogy to the core-level case.[15] On the basis of these arguments we propose a three-parameter model for estimating the relaxation energies of all the MO's of the fluorinated methanes. We assume, for simplicity, that all "F 2s-like" orbitals have one mean value of E_R, that all other orbitals have another, and the E_R^{ea} is the same for all orbitals within a given molecule, but that it rises linearly with the number of fluorines (this crudely expresses the molecular size dependence). After the $\Delta\varepsilon_{ai}$ values in Table I have been used to adjust parameters, the expressions for E_R are

$$E_R = (4.5 + 0.5\ n)\ \text{eV} \tag{6}$$

for F 2s-like orbitals, and

$$E_R = (1.0 + 0.5\ n)\ \text{eV} \tag{7}$$

for all other orbitals, where n is the number of fluorines. In applying these equations we again assume for simplicity that a given orbital is either entirely or not at all F 2s-like, even though there is correlation between the amount of F 2s character and E_R in several orbitals

that have small admixtures of 2s character. With this approach we have estimated the "theoretical" values $E_B(\text{theo}) = -\varepsilon - E_R$ given in Table I. The agreement between $E_B(\text{theo})$ estimated in this way and $E_B(\text{expt})$ is on the whole excellent, as Fig. 2 shows. For the 33 orbitals studied the standard and mean deviations between $E_B(\text{theo})$ and $E_B(\text{expt})$ are 0.48 eV and 0.27 eV, respectively. This figure also shows the marked separation between E_B values of the F 2s-like orbitals and those of the other molecular orbitals in these molecules. We conclude that relaxation corrections of the type described here are both conceptually and pragmatically superior to simply reducing the orbital energies by a constant factor, although of course our approach has been an empirical fitting procedure rather than a predictive calculation.

Intensities and Spectroscopic Assignments

In order to apply the intensity model outlined above, a knowledge of the relative atomic cross section is needed. Thus, to interpret the fluoromethane data the ratios

$\sigma(C2s)/\sigma(C2p)$, $\sigma(F2s)/\sigma(F2p)$ and $\sigma(F2s)/\sigma(C2s)$ are

required. Gelius obtained the first of these three quantities from the experimental XPS area ratios of methane ($2a_1$ and $1t_2$) and an *ab initio* calculation. Similarly, the last ratio was obtained from the $4a_1$ and $3t_2$ levels of CF_4. The $\sigma(F2s)/\sigma(F2p)$ ratio was interpolated due to the unavailability of a spectrum of either HF or F_2. In our case, the $\sigma(C2s)/\sigma(C2p)$ was similarly calculated from the $2a_1$ and $1t_2$ of methane. However, we chose instead to use the $3a_1$ and $4a_1$ levels

of CH_3F for the $\sigma(F2s)/\sigma(C2s)$, since they have predominantly fluorine s and carbon s character, respectively. The $\sigma(F2s)/\sigma(F2p)$ ratio was obtained from the 2σ and $1\pi_x$, $1\pi_y$ orbitals of HF (Fig. 1). Gelius used gross populations in calculating his ratios. Since his model neglects the contributions to the cross section from electrons far from the nuclei, it seems more appropriate to employ net populations instead. We have computed ratios using both types of populations. The results are shown in Table II.

It is clear from Table II that the cross section ratios are not independent of the theoretical method used. Furthermore, it is interesting to note that in the case of the $\sigma(C2s)/\sigma(C2p)$ ratio, the type of population used (net or gross) seems to be more important than the quality of the calculation (semi-empirical or ab initio).

The relative molecular orbitals intensities calculated from POLYATOM and CNDO/2 populations (using Eqs. (1) and (2) and the cross section ratios from Table II) are compared with experiment in Table III and are shown as vertical bars (using POLYATOM net populations) in Fig. 1. Their positions have been adjusted to match those of the experimental peaks. Some fitting of the spectra is shown in Fig. 1. Expanded spectra of the low binding-energy regions of the fluorinated methanes are shown in Fig. 3 (with relative intensity calculated using CNDO/2 populations). As stated earlier, our measurements were made using a right angle geometry of x-ray to photoelectron beams. The relative intensities should change as the angle is altered. In fact, angular distribution studies constitute an important diagnostic tool for probing orbital parentage.[17] Individual spectroscopic assignments

are discussed below.

CH_4

It is unfortunate that the $K\alpha_3$ and $K\alpha_4$ satellites of the exciting Mg radiation obscure the $1t_2$ peak in methane. The situation is not quite so bad with Aℓ x-rays because the satellites are farther from the $K\alpha_{1,2}$ line. Nonetheless, this has resulted in a large uncertainty in the $2a_1/1t_2$ area ratio. In Fig. 1 the $1t_2$ region of the Aℓ $K\alpha_{1,2}$ XPS spectrum is reproduced using a Jahn-Teller splitting of 0.8 eV and a 2 to 1 intensity ratio of the Jahn-Teller components.[18] These are the values seen in UPS studies.[8]

CH_3F

The ordering of $5a_1$ and 1e has been uncertain. Both CNDO and POLYATOM yield a lower binding energy for $5a_1$. The calculated intensities all agree that 1e is somewhat more intense. The experimental peak is asymmetric on the high binding energy side indicating the location of the smaller peak. This is seen most clearly in Fig. 3. Thus, Gelius model seems to favor placing 1e at a lower binding energy than $5a_1$.

CH_2F_2

The $2b_1$ and $3a_1$ orbitals are reported here for the first time. The level ordering indicated by orbital energies is supported by the intensity ratios. The remaining peaks are shown in more detail in Fig. 3. In the case of the two lowest binding energy groups of peaks, our analysis of the peaks in Fig. 3 is based on the calculated CNDO intensities which give a good overall fit of the experimental data.

The experimental ratio of the $1a_2$, $4b_1$, $6a_1$ peak area to that of the $2b_2$ peak is approximately 5:1. This is to be compared to a ratio of 3:1 in the He II spectrum.[8] The increase in the relative intensities over the statistical value can be understood in terms of our model as follows: the orbitals $1a_2$ and $4b_1$ do not have any hydrogen character by symmetry. The $6a_1$ has less contribution from hydrogen than does $2b_2$.[9] Thus, in all four orbitals most of the electron density is on the fluorines, mainly in the 2p levels; and the ($1a_2$ + $4b_1$ + $6a_1$) peak has a larger percentage of electrons on the fluorines than does $2b_2$.

In the next peak, at ∿19 eV, there are three orbitals. The ordering of $3b_1$ and $5a_1$ may be reversed without disagreeing with our spectrum. However, it seems quite likely that $1b_2$ has a higher binding energy than both of them, as shown, because its low intensity is consistent with the asymmetry of this peak on the high-energy side.

CHF_3

The ab initio and CNDO calculations together with the Gelius model place $3a_1$ unambiguously as the most tightly bound MO. The model also seems to indicate that 3e is less tightly bound than $5a_1$ (Fig. 3). This is in agreement with Brundle et al.[8] who relied on the Koopmans' theorem energies. We also propose in Fig. 3 an ordering for the four outer orbitals which is predicted by POLYATOM.[9] This fit was obtained using the reported UPS vertical ionization potentials and the area ratios calculated from CNDO. The ordering of 5e and $1a_2$ is reversed by CNDO. On the basis of intensity ratios our spectra establish the ordering of these four levels as shown in Fig. 3.

CF_4

Siegbahn[19] has studied the CF_4 spectrum with monochromatized x-rays. His results as well as ours show that the least-bound orbital is more intense than the next one. According to the cross-section ratios obtained from both POLYATOM and CNDO/2 populations, $1t_1$ should be the least-bound orbital (see Table III) as predicted by ab initio calculations. Thus comparison with our experimental intensities very slightly favors $1t_1$ as the most weakly bound orbital.

Trends Through the Series

Some interesting binding-energy correlations can be made through the fluoromethane series. For example, Brundle et al.[8] noted that the energies of the $4a_1$ orbitals increase linearly with fluorination. These orbitals show strong C-H overlap (see Table III of Ref. 8). The total C-H overlap (P_{C-H}) of $4a_1$ is plotted against our experimental $4a_1$ binding energies in Fig. 4. For CH_4 the corresponding level is $2a_1$. Substitution of fluorines for hydrogens results in a migration of electron population from the C-H region toward the fluorines, thus increasing the $4a_1$ binding energies. At the same time the populations of the remaining C-H bonds are left essentially intact. Additivity of inductive effects in the fluoromethanes and other compounds has been observed elsewhere.[20]

The $3a_1$ orbital is C-F bonding and a plot of total overlap populations[9] versus $3a_1$ binding energy is also shown in Fig. 4. The C-F bonding population for a single bond decreases through the series $CH_3F \rightarrow CF_4$, but the total bonding population shows an almost linear

increase with the binding energy of the $3a_1$ orbital.

The $2b_1$ level of CH_2F_2, 2e of CHF_3, and $2t_2$ of CF_4 can be grouped together. The variation in their binding energies, which increase by 1 eV for the substitution of a hydrogen by a fluorine, correlates linearly with the F 2s populations (gross or net) of these orbitals. This is shown in Table IV.

These linear relationships extend the concept of "group shifts", which could be expressed by the relation[21]

$$\Delta E = \sum_{\text{group}} (\Delta E_{\text{group}} - \Delta E_H) \quad .$$

Furthermore, the point-charge potential concepts that led to this equation for core levels is clearly not viable here: the slopes $\Delta E(\text{C 1s})/\Delta E(4a_1)$ are not compatible with such a model, for example. Bond energies would have to be explicitly taken into account to explain the slopes in Fig. 4. Further interpretation of these linear relationships would be outside the scope of this paper. We wish simply to note their existence and to observe that they are consistent with chemical intuition.

References

1. D. W. Turner, C. Baker, A. D. Baker, and C. R. Brundle, Molecular Photoelectron Spectroscopy, (Wiley-Interscience, London, 1970).
2. K. Siegbahn, C. Nordling, G. Johansson, J. Hedman, P. F. Heden, K. Hamrin, U. Gelius, T. Bergmark, L. O. Werme, R. Manne, and Y. Baer, ESCA Applied to Free Molecules, (North-Holland, Amsterdam, (1969).
3. U. Gelius in Electron Spectroscopy, D. A. Shirley, ed., (North-Holland, Amsterdam, 1972).
4. R. S. Mulliken, J. Chem. Phys. 23, 1833 (1955).
5. (a) C. S. Fadley, S. B. M. Hagstrom, M. P. Klein, and D. A. Shirley, J. Chem. Phys. 48, 3779 (1968);
   (b) D. W. Davis, D. A. Shirley, and T. D. Thomas, J. Amer. Chem. Soc. 94, 6565 (1972).
6. A neon 2s value of 48.47 eV has been reported recently. See G. Johansson, J. Hedman, A. Berndtsson, A. Klasson, and R. Nilsson, J. Electr. Spectr. 2, 295 (1973).
7. C. R. Brundle, Chem. Phys. Letters 7, 317 (1970).
8. C. R. Brundle, M. B. Robin, and H. Basch, J. Chem. Phys. 53, 2196 (1970).
9. L. C. Snyder and H. Basch, Molecular Wave Functions and Properties, (John Wiley and Sons, New York, 1972).
10. J. W. D. Connolly, H. Siegbahn, U. Gelius, and C. Nordling, J. Chem. Phys. 58, 4265 (1973), and references therein.
11. K. H. Johnson, J. Chem. Phys. 45, 3085 (1966); K. H. Johnson and F. C. Smith, Jr., Phys. Rev. B 5, 831 (1972).

12. T. Koopmans, Physica 1, 104 (1933).

13. P. S. Bagus, Phys. Rev. 139, A619 (1965).

14. D. A. Shirley, Chem. Phys. Letters 16, 220 (1972).

15. D. W. Davis and D. A. Shirley, Chem. Phys. Letters 15, 185 (1972).

16. (a) S. P. Kowalczyk, F. R. McFeely, R. A. Pollak, and D. A. Shirley, Phys. Rev. B 8, 2387 (1973);

(b) L. Ley, S. P. Kowalczky, F. R. McFeely, R. A. Pollak, and D. A. Shirley, Phys. Rev. B 8, 2392 (1973).

17. A. E. Jones, K. Schweitzer, F. A. Grimm, and T. A. Carlson, J. Electron Spectrosc. 1, 29 (1972-73).

18. See for example, C. A. Coulson and H. L. Strauss, Proc. Roy. Soc. (London) A 269, 443 (1962) and ref. 8.

19. K. Siegbahn, in Atomic Physics 3, Proceedings of the Third International Conference on Atomic Physics, Boulder, Colorado, 1972, edited by S. J. Smith and G. K. Walters (Plenum, New York, 1973), p. 493. Also K. Siegbahn, University of Uppsala, Report No. UUIP-793 (Uppsala University Institute of Physics, Uppsala, 1972).

20. D. W. Davis, M. S. Banna, and D. A. Shirley, J. Chem. Phys. 60, 237 (1974).

21. D. A. Shirley, in Advances in Chemical Physics, Vol. 23, (I. Prigogine and Stuart A. Rice, editors), p. 85 (1973).

Table I. Molecular Orbital Binding Energies in Fluorinated Methanes (in eV).

Molecule	Orbital	E_B(XPS)[a]	E_B(UPS)[b]	$-\varepsilon_{ab\ initio}$	$-\varepsilon_{CNDO/2}$	$\Delta\varepsilon_{ai}$	E_B(theo)
CH_4	$1t_2$	14.2(2)[c]	14.0	14.74	19.79	0.6	13.74
	$2a_1$	23.05(2)	23.0	25.68	34.54	2.63	24.68
CH_3F	2e	13.31(4)	13.05	14.43	17.57	1.12	12.93
	1e	16.85(7)	~17.0	18.00	21.28	1.15	16.50
	$5a_1$	17.56(9)		18.89	24.12	1.33	17.39
	$4a_1$	23.48(3)	23.4	26.13	32.06	2.65	24.63
	$3a_1$	38.41(3)	-	43.17	47.10	4.76	38.17
CH_2F_2	$2b_2$	13.17[d,e]	13.27	14.89	17.11	1.72	12.89
	$6a_1$	14.91[e]		16.94	18.88	2.03	14.94
	$4b_1$	15.20[d,e] (2)	15.3	17.23	19.82	2.03	15.23
	$1a_2$	15.61[d,e]	15.71	18.22	21.38	2.61	16.22
	$3b_1$	18.51(4)[e]		20.38	23.96	1.87	18.38
	$5a_1$	19.07(3)[e]	18.9	21.13	25.23	2.06	19.13
	$1b_2$	19.76(7)		21.54	26.97	1.78	19.54
	$4a_1$	23.86(3)	23.9	26.77	31.15	2.91	24.77
	$2b_1$	38.20(7)	-	43.79	45.82	5.59	38.29
	$3a_1$	40.13(7)	-	45.63	50.15	5.50	40.13
CHF_3	$6a_1$	14.67[d,e]	14.80	16.53	17.77	1.86	14.03
	$1a_2$	15.29[d,e]	15.5	18.33	21.52	3.04	15.83
	5e	15.99[d,e] (4)	16.2	18.54	19.94	2.55	16.04
	4e	17.03[d,e]	17.24	19.71	22.24	2.68	17.21

(continued)

Table I. (continued)

Molecule	Orbital	E_B(XPS)[a]	E_B(UPS)[b]	$-\varepsilon_{ab\ initio}$	$-\varepsilon_{CNDO/2}$	$\Delta\varepsilon_{ai}$	E_B(theo)
	3e	20.25(3)	20.6[f]	22.87	26.35	2.62	20.37
	$5a_1$	20.89(3)		23.78	27.86	2.89	21.28
	$4a_1$	24.38(3)	24.44	27.49	30.88	3.11	24.99
	2e	39.15(4)	-	45.34	47.20	6.19	39.34
	$3a_1$	42.03(9)	-	48.22	52.78	6.19	42.22
CF_4	$1t_1$	16.23(3)	16.20	19.40	22.24	3.17	16.40
	$4t_2$	17.41(4)	17.40	19.65	20.20	2.24	16.65
	1e	18.43(4)	18.50	21.34	23.30	2.91	18.34
	$3t_2$	22.14(2)	22.12	24.89	28.18	2.75	21.89
	$4a_1$	25.11(2)	25.12	28.15	29.48	3.04	25.15
	$2t_2$	40.30(4)	-	46.65	48.22	6.35	40.15
	$3a_1$	43.81(10)	-	50.50	54.63	6.69	44.00
HF	1π	16.12(4)	16.04	17.50	21.28		
	3σ	19.89(7)	19.90	20.50	23.14		
	2σ	39.65(2)	-	43.61	45.55		

[a] Binding energies using Mg Kα x-rays except with CH_4 where Al Kα x-rays were used.

[b] Vertical binding energies from Ref. 8.

[c] Weighted average of Jahn-Teller levels

[d] Separations from UPS used.

[e] Area ratios from CNDO/2 used.

[f] This value is probably correct. The value given in Ref. 8 is 19.84 eV for the vertical IP and 20.6 eV for the adiabatic IP.

Table II. Calculated Relative Atomic Photoelectric Cross Sections

Ratio	CNDO	POLYATOM (Net)[b]	POLYATOM (Gross)[b]	Gelius[a]
$\sigma(C2s)/\sigma(C2p)$	23.3[c]	19.9	19.2[c]	13
$\sigma(F2s)/\sigma(F2p)$	9.5[d]	10.3[d]	9.1[d]	10
$\sigma(F2s)/\sigma(C2s)$	8.0[e]	5.8[e]	4.1[e]	2

[a] Ref. 3

[b] Wavefunctions and overlaps obtained from Ref. 9.

[c] Using relative areas of $2a_1$ and $1t_2$ orbitals of methane.

[d] Using relative areas of 2σ and 1π orbitals of hydrogen fluoride.

[e] Using relative areas of $3a_1$ and $4a_1$ orbitals of methyl fluoride.

Table III. Computed Molecular Orbital Intensity Ratios from CNDO and POLYATOM Calculations.

Molecule	Molecular Orbital	I^{a}_{CNDO}	I^{b}_{NP}	I^{c}_{GP}	I_{exp}
HF	1Π	0.24	0.24	0.24	0.24(2)
	3σ	0.14	0.20	0.16	0.19(3)
	2σ	1.00	1.00	1.00	1.00(2)
CH_4	$1t_2$	0.12	0.12	0.12	0.12[d](2)
	$2a_1$	1.00	1.00	1.00	1.00(3)
CH_3F	2e	0.14	0.12	0.11	0.13(1)
	1e	0.14	0.14	0.15	0.11(2)
	$5a_1$	0.12	0.11	0.11	0.08(2)
	$4a_1$	0.24	0.23	0.26	0.23(1)
	$3a_1$	1.00	1.00	1.00	1.00(3)
CH_2F_2	$2b_2$	0.058	0.064	0.065	0.05[e,f] } (1)
	$6a_1$	0.089	0.10	0.11	0.07[e] } (1)
	$4b_1$	0.11	0.12	0.11	0.09[e,f] } (1)
	$1a_2$	0.12	0.12	0.12	0.09[e,f] } (1)
	$3b_1$	0.14	0.16	0.15	0.08[e] } (1)
	$5a_1$	0.14	0.10	0.11	0.08[e] } (1)
	$1b_2$	0.062	0.055	0.063	0.04[e] } (1)
	$4a_1$	0.24	0.32	0.26	0.28(1)
	$2b_1$	1.00	1.00	1.00	1.00(6)
	$3a_1$	0.84	0.85	0.93	0.89(5)

(continued)

Table III. (continued)

Molecule	Moleculear Orbital	I^{a}_{CNDO}	I^{b}_{NP}	I^{c}_{GP}	I_{exp}
CHF_3	$6a_1$	0.038	0.049	0.042	$0.03^{e,f}$
	$1a_2$	0.062	0.064	0.071	$0.05^{e,f}$
	5e	0.12	0.12	0.12	$0.09^{e,f}$ (1)
	4e	0.12	0.12	0.13	$0.09^{e,f}$
	3e	0.18	0.19	0.15	0.09(1)
	$5a_1$	0.12	0.048	0.052	0.06(1)
	$4a_1$	0.10	0.20	0.15	0.18(1)
	2e	1.00	1.00	1.00	1.00(3)
	$3a_1$	0.43	0.40	0.48	0.42(2)
CF_4	$1t_1$	0.13	0.14	0.14	0.12(1)
	$4t_2$	0.12	0.13	0.12	0.11(1)
	1e	0.083	0.080	0.086	0.08(1)
	$3t_2$	0.20	0.23	0.17	0.17(1)
	$4a_1$	0.11	0.16	0.12	0.16(1)
	$2t_2$	1.00	1.00	1.00	1.00(3)
	$3a_1$	0.28	0.26	0.31	0.29(2)

[a] Relative intensity using CNDO populations.

[b] Relative and intensity using POLYATOM net populations calculated from ref. 9.

[c] Relative intensity using POLYATOM gross populations calculated from ref. 9.

[d] Assuming one level, not Jahn-Teller split.

[e] Area ratios taken from CNDO.

[f] Separations taken from UPS.

Table IV. F2s Binding Energies and Populations for the Next-To-Innermost Molecular Orbital of CH_2F_2, CHF_3, and CF_4

Molecule	Orbital	Binding Energy(eV)	Gross Population*	Net Population*
CH_2F_2	$2b_1$	38.20	1.87	1.22
CHF_3	2e	39.19	3.65	2.36
CF_4	$2t_2$	40.18	5.37	3.45

*Calculated from ref. 9.

Figure Captions

Fig. 1. X-ray photoelectron spectra of HF and the fluoromethane series $CH_{4-n}F_n (0 \leq n \leq 4)$ taken at increments of ∿0.33 eV. Vertical bars correspond to intensity ratios computed using POLYATOM net populations.[9] They are not corrected for the consideralbe variation in line width. In some cases, noted in Table I, separations from UPS and/or intensity ratios from CNDO/2 were used. For CH_2F_2 two groups of levels were fit as two peaks.

Fig. 2. Plot of binding energies calculated from a three-parameter model versus experimental values.

Fig. 3. X-ray photoelectron spectra of the fluoromethanes in the region up to approximately 30 eV binding energy taken at increments of ∿0.16 eV. Vertical bars correspond to computed intensity ratios using CNDO/2 populations. In some cases separations and intensity ratios were used as explained for Fig. 1.

Fig. 4. Variation of total C-F overlap population of $3a_1$ and total C-H overlap population of $4a_1$ ($2a_1$ in methane) with binding energies of $3a_1$ and $4a_1$, respectively. Overlap populations were obtained from refs. 8 and 9.

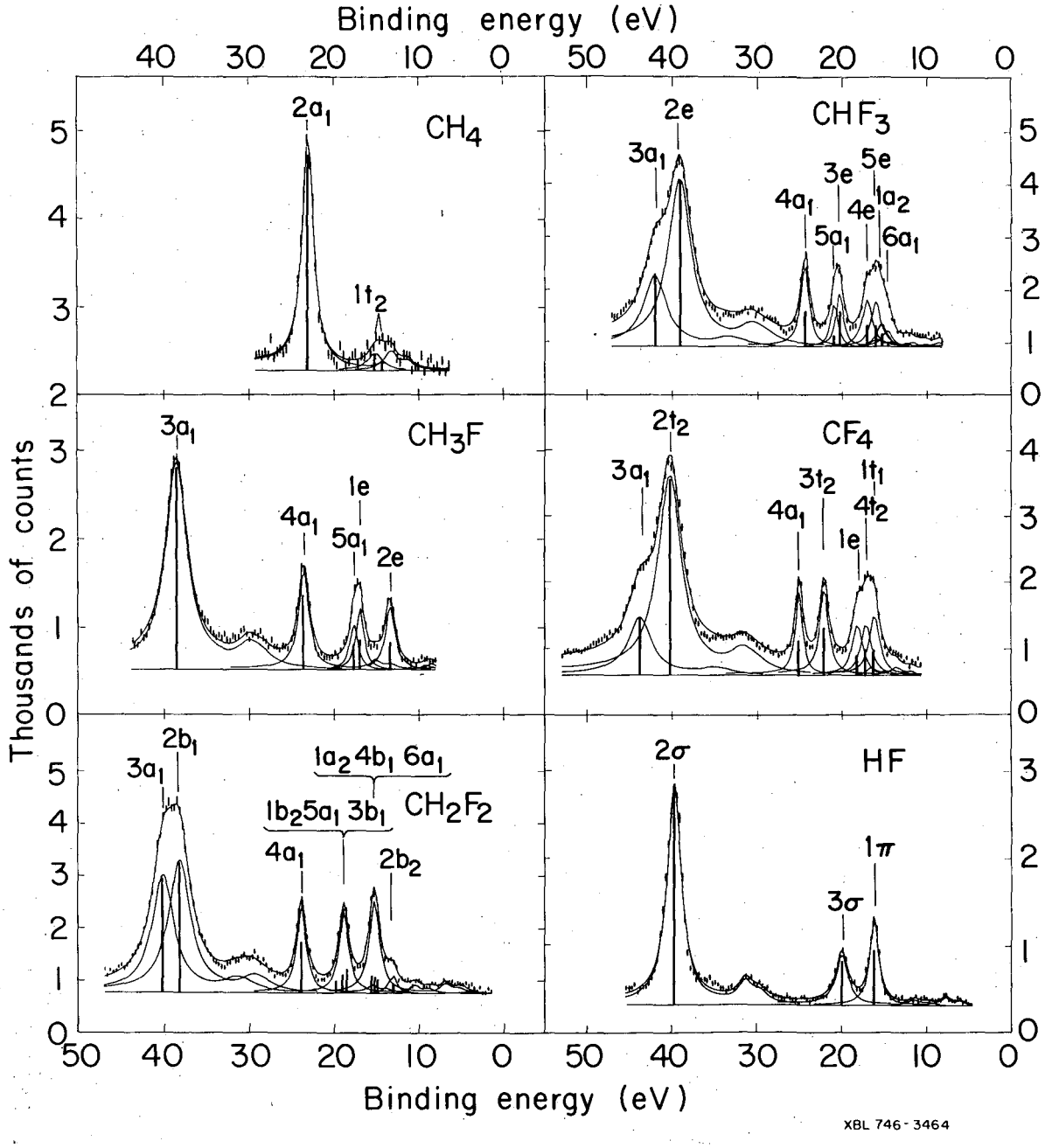

Fig. 1

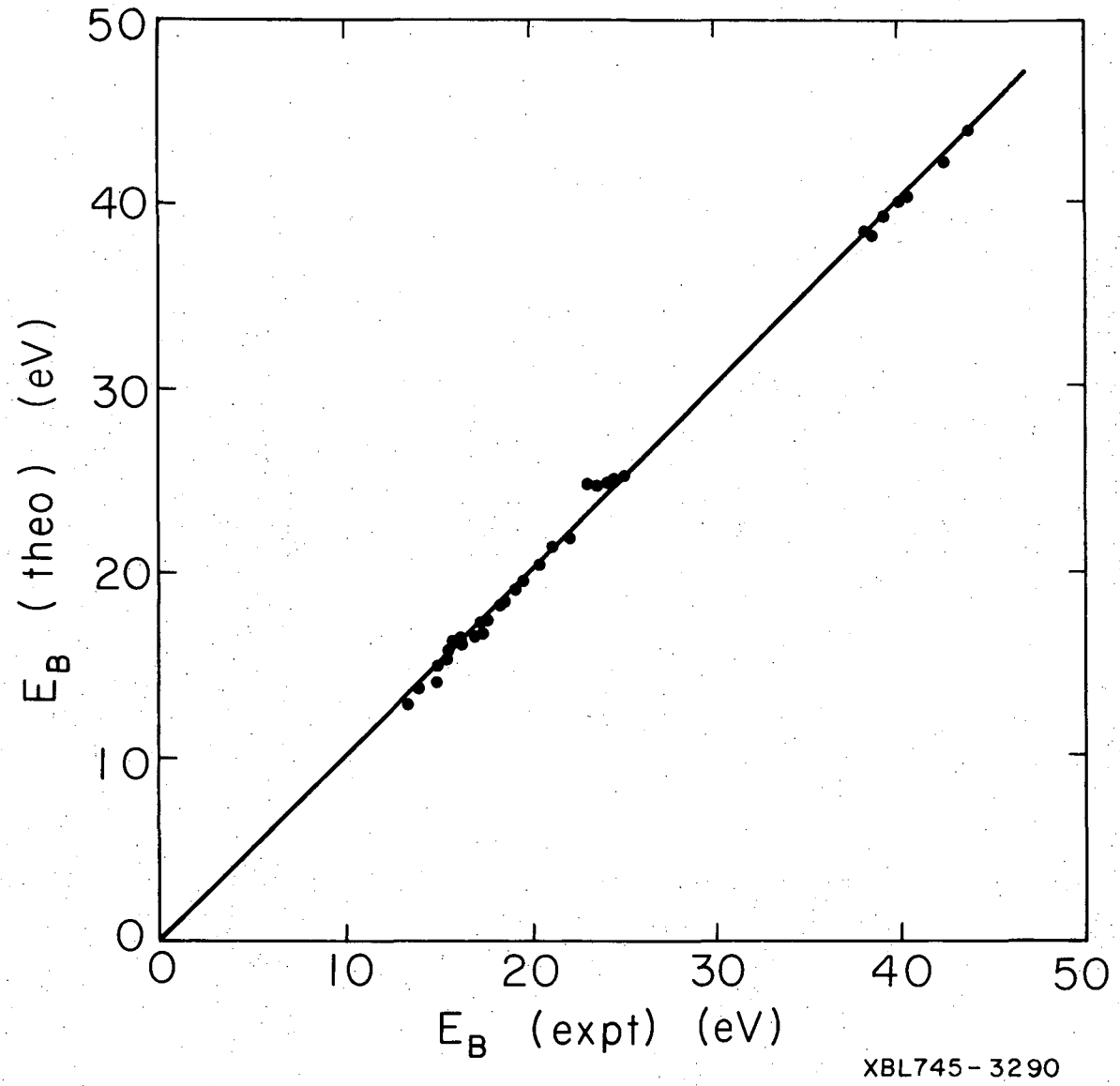

Fig. 2

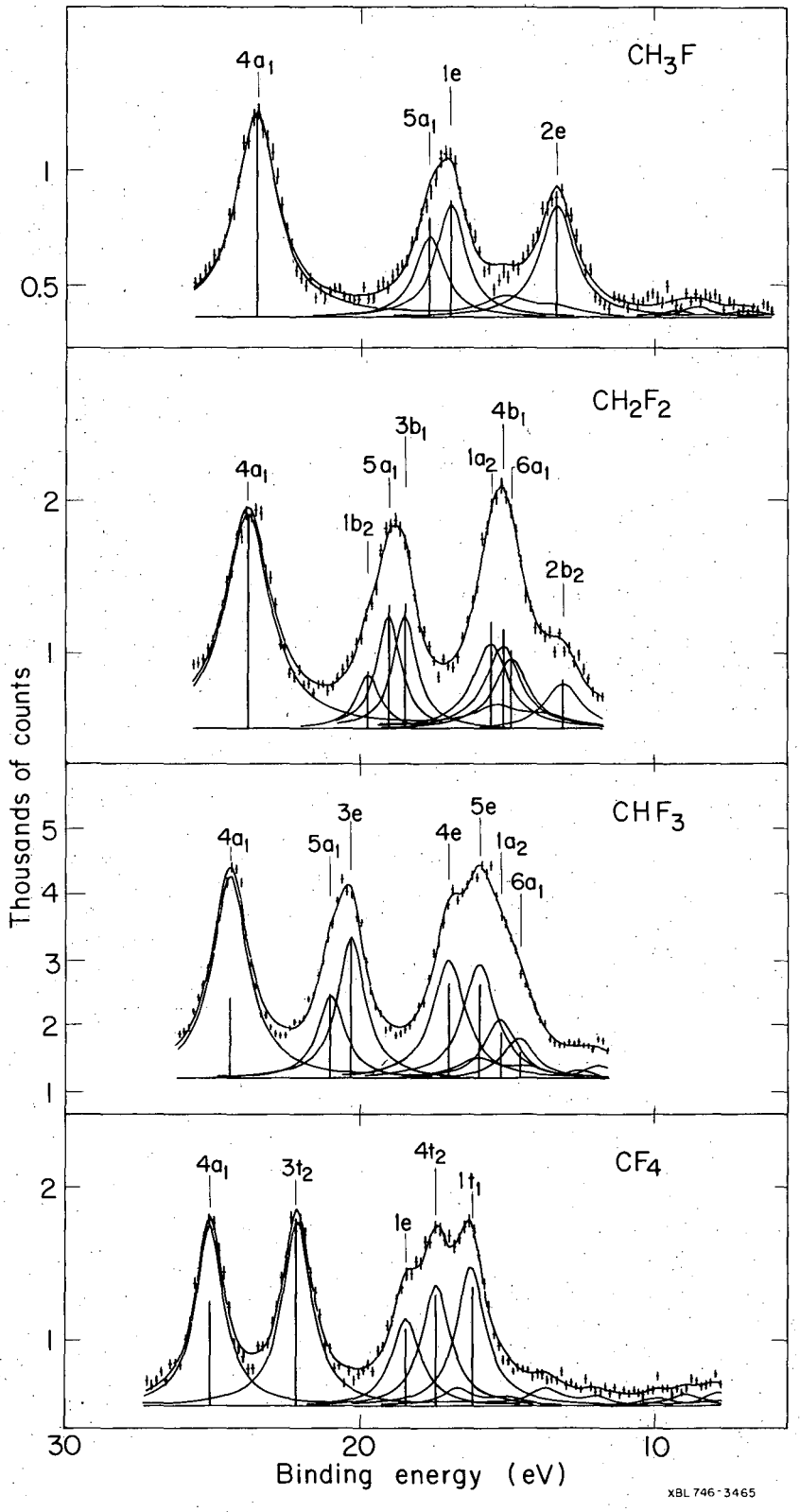

Fig. 3

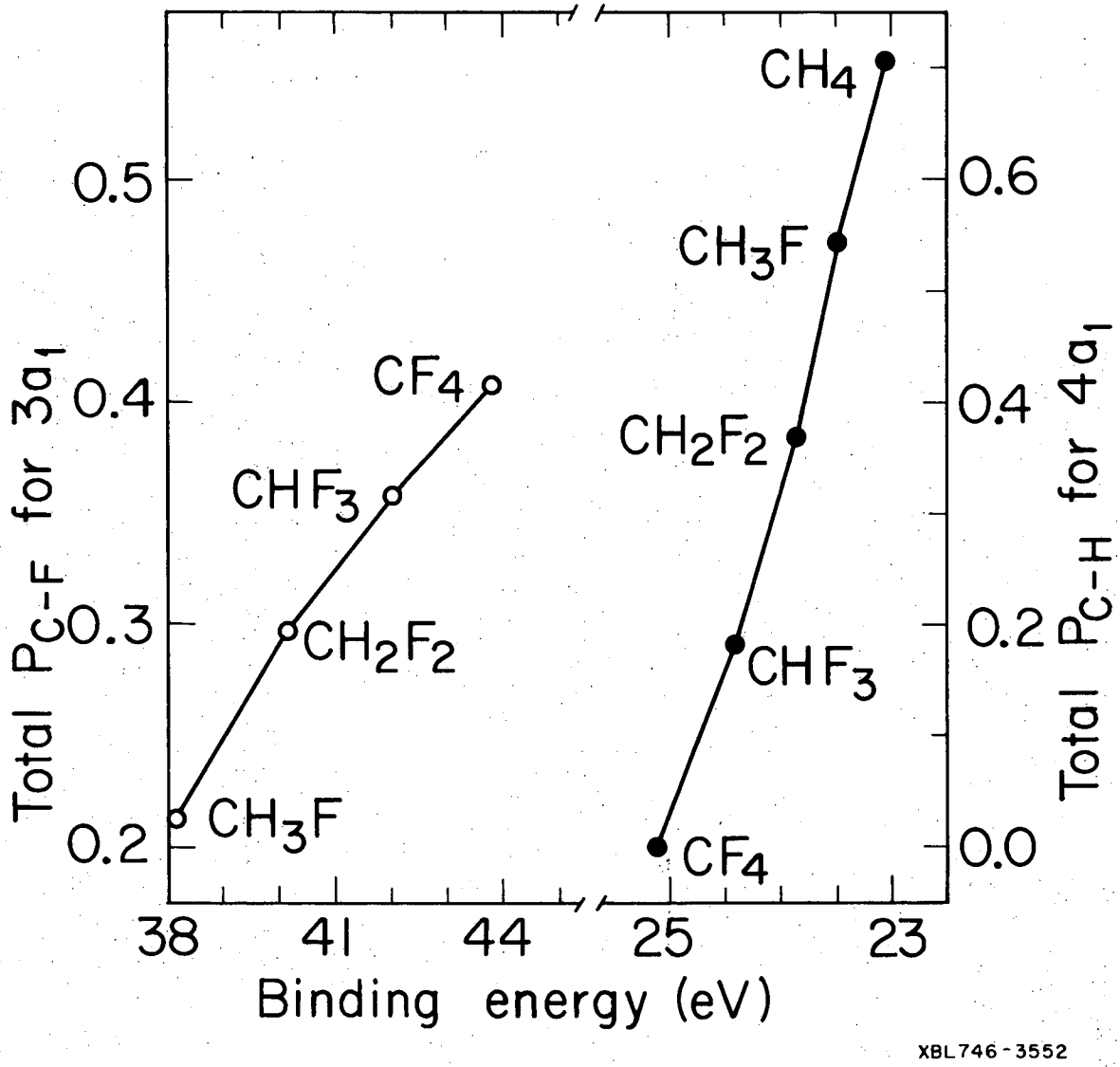
CH4
CH3F
CH2F2
CHF3
CF4
CF4
CHF3
CH2F2
CH3F
0.5
0.4
0.3
0.2
0.6
0.4
0.2
0.0
38
41
44
25
23
Binding energy (eV)
Total PC-F for 3a1
Total PC-H for 4a1
XBL746-3552

Fig. 4

IV. XPS OF THE 2s REGION OF CYCLIC HYDROCARBONS IN RELATION TO AMORPHOUS GROUP IV AND V ELEMENTS

Abstract

Ge, Si, As, Sb, and Bi display a characteristic two band structure in the x-ray photoelectron spectra of their s-like valence bands. In the corresponding amorphous materials, however, the gap between these two bands is filled in. It has been suggested that this is the result of the existence of odd-membered rings (specifically 5-membered rings) in the amorphous cases while the crystalline solids contain only 6-membered rings. This is supported by the radial distribution function of certain of the amorphous materials which indicates uniform bond lengths but variations in bond angles.

Experimentally it is possible to obtain pure tetrahedrally bonded systems of different ring sizes in the gas phase cyclic hydrocarbons. The XPS spectrum of cyclohexane shows a striking resemblance to that of diamond--if the cyclohexane spectrum is broadened by 0.8 eV, they are almost identical. The other gas phase spectra can be similarly broadened and then added together according to different ring structure models. When this is done, the conclusion is that 5- and 6-membered rings alone are not sufficient to explain the "filling-in effect" but 5-, 6-, and 7-membered rings are.

Introduction

The valence band x-ray photoelectron spectra of amorphous Ge, Si, As, Sb, and Bi display certain differences from the analogous spectra of their crystals.[1,2] Ge, Si, and As are shown in Fig. 1. One of the more striking differences is that peaks 1 and 2 in the cleaved crystal spectra are replaced by a broad band in the amorphous case. These levels arise primarily from atomic 5-like orbitals. As the atoms come together to form the solid, these levels are split by interactions with other atoms to form bands. The fact that these bands are different in the crystalline and amorphous cases could be due to either long range disorder, short range disorder, or a combination of both.

At standard temperature and pressure Ge and Si have the diamond crystal structure. The atoms are tetrahedrally bonded (sp^3) to form connected chair-form six-membered rings. The group V elements (s^2p^3) have an A-7 crystal structure--more complex than diamond, but also composed of six-membered rings. Of course, Ge and Si have been more intensely studied. It is known that they can be prepared in the amorphous form with approximately the same density as in the crystalline form.[3] Radial distribution function measurements of Ge, for example, give a first-neighbor (bond-length) distance which is nearly constant (±0.04 Å), whereas there is a rather large variation in second-neighbor distance of ±0.25 Å, indicating bond angle variations. Furthermore, the third-neighbor peak is not well defined.[4] This indicates short-range disorder and would tend to rule out a microcrystalline model of the structure and any amorphous cluster model

in which angles do not change. The requirements of fixed bond length and angular variation are met by continuous random network model which can be infinite at the expense of local distortion. This last structure does not require discontinuities as between micro-crystals or clusters and can thus be constructed to have a density as high or nearly as high as the crystalline density, in agreement with experiments on defect-free samples.

One of the more interesting structural features of the continuous random network model is that it can be constructed so as to have non-six-membered rings. Polk,[5] in counting the rings in his model, noted that there were 20% five-membered rings. It has been suggested that such rings could have significant effect on the s-like valence band spectra of these amorphous materials. This is because these elements are covalently bonded with localized orbitals and the s-levels, which are basically atomic, are sensitive to their local environment rather than to the crystal as a whole. Joannopoulos and Cohen[6] have suggested a model for local disorder which is amenable to band-structure computations. This is the ST-12 high-pressure structure of Ge III[7] and ice III,[8] with 12 atoms per simple tetragonal unit cell. Eight of the atoms form two spirals with the other atoms connecting the spirals. There is very little bond length variation, but the bond angles vary from 91 to 120 degrees in Ge III (a much larger variation than in amorphous samples). In addition, the structure contains 5-, 6-, 7-, and 8-membered rings. Calculations on Ge III indicate a "filling-up" of the gap between the two s-like valence bands; just what is seen

in the amorphous valence band spectra.

In order to definitely ascribe the change in valence band spectra to ring size, one would like to be able to study covalent tetrahedral compounds of various ring sizes. Unfortunately, a crystal lattice of, for example, symmetrical interconnecting five-membered rings is impossible. However, a series of covalent tetrahedral molecules of every ring size exists--the cyclic alkanes. We shall use these hydrocarbons as model compounds because of their availability and their enhancement of the spectral region of interest (to be discussed in the next section). Amorphous carbon is not, of course, on the list of elements showing the effect we are investigating because the thermodynamically stable form of carbon at room temperature and pressure is graphite (sp^2), not diamond (sp^3). Through the use of the cyclic alkanes we hope to check the hypothesis that the s-like valence band spectrum reflects the local ring sizes in tetrahedrally bonded solids.

Experimental

Photoelectron spectra were taken on the 50 cm. radius Berkeley magnetic spectrometer at a sample pressure of about 100 Torr. Cyclopentane, cyclohexane, cycloheptane, and cyclooctane spectra were taken with Mg Kα x-rays (Fig. 2) at energy increments of about 0.16 eV. All compounds were also run using Aℓ Kα x-rays at energy increments of about 0.18 eV--the spectra were identical within experimental error.

At first glance it is not obvious how the spectra in Fig. 1 are related to those in Fig. 2. The energy scale, for example, seems quite different. Part of the reason for this is that solid spectra

are referenced to the Fermi level, whereas energy levels in a gas are plotted relative to the vacuum level and first ionization potentials in hydrocarbons are about 10 eV. In addition, the total width of the valence region in the carbon compounds is considerably greater than for the other species. This is a general rule for first row elements.

X-ray photoelectron spectra of first row elements also have intensity effects caused by the fact that the 2s wavefunction has a radial node while the 2p does not. The result of this is that the overlap of a 2s orbital with the wavefunction of the departing photoelectron (de Broglie λ = 0.35 Å) is more than an order of magnitude greater than that of a 2p orbital. For this same reason, H 1s levels cannot be seen. Naturally, this does not apply to second and subsequent rows where both types of orbitals have radial nodes. The p-like levels in Fig. 2, between 10 and 17 eV, are barely visible, whereas the levels of interest, the s-like ones, are well defined. Also, the peaks in the spectrum are obviously almost pure s or p with very little mixing. This seems to be the case in the solids,[11] too, where these is a definite dip in intensity between the first p-like bands and the double-peak s-like bands.

In order to show that cyclohexane is a good model compound for diamond the two spectra are shown in Fig. 3 with the energy scale on diamond[11] shifted to roughly correspond to the cyclohexane spectrum. Also shown is $C(CH_3)_4$ (neopentane) to illustrate that simply having tetrahedral carbon bonds is not sufficient for simulating diamond. If one takes each data point in the cyclohexane spectrum and "broadens"

it by 0.8 eV (to reflect the interaction of the rings in the solid), the resulting sum of these broadened data points, seen on the top of Fig. 4, is almost identical to the diamond spectrum.

Theoretical

In order to understand the reasons for the different level energies in the various ring compounds, we have performed several calculations. On the simplest level we can make use of the facts that the atomic C 2s orbitals are symmetric and that each s orbital has the same interaction with its neighboring C 2s orbitals every other one. Therefore, to a first approximation, we can treat an N-membered ring as belonging to the group C_n and treat it as we would an aromatic π system. The only difference is that each level in this case is filled. The energy levels can be found using the formula

$$E_n = \alpha + 2\beta \cos \frac{2n\pi}{N}, \qquad n = 0, 1, \ldots, N-1,$$

where α is the 2s energy of an isolated carbon atom and β is the interaction between neighboring C 2s orbitals. Both α and β are intrinsically negative.[12] Each of the ring systems has one deepest singly degenerate a level followed by e levels. In the case of even-membered rings, the last level is again singly degenerate. For a 6-membered ring this gives two singly degenerate levels at $E = \alpha + 2\beta$ and $\alpha - 2\beta$. Between them are two doubly degenerate (e) levels at $E = \alpha + \beta$ and $\alpha - \beta$. The two e levels are separated by 2β, while the other levels are separated from the e levels by β. This leads to a dip at α. Similarly there are dips at -0.5α, 0.4α and -1.12α, and $\pm.7\alpha$ for 5-, 7-, and 8-membered rings, respectively. In addition we

see that the deepest level in each case has an energy of $\alpha + 2\beta$ while the least-bound level has an energy of at least $\alpha - 2\beta$. That is, all of the bands fall within the bounds of the energy space spanned by the 6-membered ring bands, so that the width of the "valence band" is not increased. This approach allows us to understand the gross features of our spectra.

In order to get a more quantitative understanding of the spectra, some calculations employing more reasonable geometries were performed.[13] First, the CNDO/2 semi-empirical method was used, the results shown in Table I along with those for other computational methods. CNDO/2 is known to give exaggerated energy eigenvalues, but it was thought that the level ordering would be useful and that the wave functions, which tend to be much better than the energies, could be successfully used to derive relative intensities. This is not the case. For example, in cyclopentane a p-type a_2'' level (not shown) is inserted between the e_2' and the e_1' and in cyclohexane the a_{2u} and e_g are reversed. The intensities are also poor. There is too much mixing of C 2s and C 2p to be consistent with experiment.

We have available the Sichel and Whitehead CNDO method[14] which is known to give better energy agreement and have tried it on this problem. Although it did not mix the s and p orbitals quite as strongly as CNDO/2, the orbital characters are quite strange. The deepest level in the odd-membered rings is an e level, not an a level which would be necessary to agree with experiment and our intuitive notion that the most stable level is the totally symmetric one. Indeed, the ordering seems to be almost precisely the reverse of that in the ab initio

GAUSS-70 calculation to be discussed below.

Disappointed in the CNDO methods, we tried extended-Hückel (EH), a semi-empirical method which is optimized for carbon compounds. The level ordering here is in perfect agreement with the ab initio results and the energies are quite good. Again, however, we see that the wave functions of the less deeply bound s-like levels are so strongly mixed with p and H 1s character that their intensity is not sufficient to reproduce the spectra.

It was necessary to use ab initio GAUSS-70 calculations to get a reasonable set of intensity ratios. These are shown in Table I.

Results and Discussion

Now that cyclohexane has been shown to be a good model for the s-like states of diamond, and if we assume diamond to be a good model for the crystalline phases of interest, we can construct "spectra" for hypothetical tetrahedrally-bonded amorphous carbon according to different structural schemes and note the effect on the valence band structure. To do this we normalize the spectra of the ring compounds and then add the individual spectra together with different weights for different ring statistics. If we then broaden these "spectra" by 0.8 eV, we get something which can be directly compared to the "crystalline spectrum" in Fig. 4a.

If we use Polk's model, where he only mentions the relative numbers of 5- and 6-membered rings, we get the "spectrum" in Fig. 4b. The minimum in the spectrum is still quite pronounced, it is simply shifted toward lower binding energy. Indeed, no matter what ratio of 5- to 6-membered rings we try, the dip merely shifts. This can be

seen in Fig. 4c where we show the result of considering only these ring numbers in the ST-12 structure. This structure has twice as many 5- as 6-membered rings. The result is the same when considering 6- and 7-membered rings only, except in this case the minimum shifts to higher binding energy.

However, if we consider 5-, 6-, and 7-membered rings, which in ST-12 appear in the ratio 2:1:2, we get the curve shown in Fig. 4d. The two s-like peaks have not broadened significantly nor has the splitting changed noticably. The gap between them has simply been filled with new levels. To proceed one step further we can consider 8-membered rings. In ST-12 there are twice as many 8-membered rings as all the smaller ones combined. Including all these, one gets Fig. 4d. These 8-membered rings do not seem necessary to describe the spectra, but considering them does not seem to interfere with the models.

The question of "short-circuiting" should be mentioned. This arises when a bridge connects two points in a ring. If a bridge contains fewer atoms than would be required to complete the original ring, the ring may be said to be "short-circuited" by a smaller ring. This is the reason Polk gave for not reporting rings larger than 6. If we apply this criterion to ST-12, however, we would have to say there are only 5-membered rings. This approach, however, might not give a representative picture of the local environment.

In conclusion we have shown that a model using odd-membered rings can be used to explain some of the experimental results on amorphous Ge, Si, As, Sb, and Bi. In particular it can explain the "filling-in"

of the gap between the two s-like peaks in the valence band XPS spectrum of the crystalline phases. These peaks seem to reflect the local bonding rather than long range effects.

References

1. L. Ley, S. Kowalczyk, R. Pollak, and D. A. Shirley, Phys. Rev. Lett. 29, 1088 (1972).
2. L. Ley, R. A. Pollak, S. P. Kowalczyk, R. McFeely, and D. A. Shirley, Phys. Rev. B8, 641 (1973).
3. See, for example, M. H. Brodsky, S. Kirkpatrick, and D. Weaire, eds. Tetrahedrally Bonded Amorphous Semiconductors, AIP Conf. Proceedings 20 (1974), and W. Paul, G. A. N. Connell, and R. J. Temkin, Adv. Phys. 22, 531, 581, 643 (1973).
4. R. J. Temkin, W. Paul, and G. A. N. Connell, Adv. Phys. 22, 581 (1973).
5. D. E. Polk, J. Non-Cryst. Solids 5, 365 (1971).
6. J. D. Joannopoulos and L. Cohen, Phys. Rev. B8, 2733 (1973).
7. F. P. Bundy and J. S. Kasper, Science 139, 340 (1963).
8. B. Kambe and Datta, Nature 187, 140 (1960).
9. K. Siegbahn in Alpha-, Beta-, and Gamma-Ray Spectroscopy, K. Siegbahn, Ed., (North-Holland Publishing Co., Amsterdam, 1965) Vol. 1, Ch. III. 5.
10. C. S. Fadley, "Core and Valence Electronic States Studied with X-ray Photoelectron Spectroscopy" (Ph.D. Thesis), Lawrence Radiaton Laboratory Report UCRL-19535 (1970), and references therein.
11. R. G. Cavell, S. P. Kowalczyk, L. Ley, R. A. Pollak, B. Mills, D. A. Shirley, and W. Perry, Phys. Rev. B7, 5313 (1973).

12. See, for example, F. A. Cotton, Chemical Applications of Group Theory, Wiley, New York, 1963.

13. Cyclopentane geometry from W. J. Adams, H. J. Geise, and L. S. Bartell, J. Amer. Chem. Soc. 92, 5013 (1970). Cyclohexane from O. Bastian, L. Fernholt, H. M. Seit, H. Kambara, and K. Kuchighu, J. Molec. Struct. 18, 163 (1973), and C-C-H angle from N. V. Alekseev and A. I. Kitaigorodskij, Z. Struct. Khim. 4, 163 (1963). Cycloheptane from D. Bocian, private communication. Cyclooctane using tetrahedral angles, tub form, and distances from smaller rings.

14. J. M. Sichel and M. A. Whitehead, Theoret. Chim. Acta. 7, 32 (1967); ibid. 11, 220 (1968).

15. W. J. Hehre, W. A. Lathau, M. D. Newton, R. Ditchfield, and J. A. Pople, GAUSSIAN 70 Program No. 236, Quantum Chemistry Program Exchange, University of Indiana, Bloomington, Indiana.

Table I. Binding Energies[a] and Intensities[b] of the s-Like Molecular Orbitals in Some Cyclic Alkanes: Theory and Experiment

LEVEL[c]	THEORY								EXPERIMENT	
	EH[d]		CNDO		SW/CNDO[e]		GAUSS 70[f]			
	E_B	I/I_o	E_B	I/I_o	E_B	I/I_o	E_B	I/I_o	E_B	I/I_o
cyclopentane										
a_1'	26.3	1.0	49.4	1.0	20.0	0.7	28.8	1.0	25.5(2)	1.0
e_2'	23.0	1.4	36.4	1.5	22.4	1.7	24.9	2.2	22.1(1)	2.0(1)
e_1'	19.0	0.7	27.1	0.8	24.8	2.0	19.7	1.9	18.4(1)	1.4(1)
cyclohexane										
a_{1g}	26.4	1.0	50.8	1.0	20.0	0.7	29.1	1.0	25.5(2)	1.0
e_u	23.8	1.6	38.7	1.7	21.8	1.6	26.0	2.2	23.2(1)	
e_g	19.9	0.9	29.7	1.0	24.3	1.9	21.1	2.1	19.7(1)	0.7(1)
a_{2u}	18.9	0.2	30.3	0.2	25.1	1.0	19.0	0.6	18.9(3)[g]	
cycloheptane[h]										
a_1'	26.4	1.0	49.1	1.0	20.1	0.6	28.7	1.0	25.1(3)[g]	1.0
$1e_2'$	24.4	1.7	40.7	1.8	21.5	1.6	26.6	2.1	23.7(1)	
e_1'	21.0	1.0	32.8	1.2	23.8	1.9	22.7	2.1	20.6(1)	0.6(2)
$2e_2'$	18.8	0.5	28.8	0.3	25.1	2.0	19.4	1.6	18.2(1)	0.5(1)
cyclooctane[i]										
a_1	26.7	1.0	54.7	1.0	20.3	0.7	29.6	1.0	25.7(2)[g]	1.0
1e	24.5	1.7	41.8	1.8	21.4	1.5	27.0	2.4	24.4(1)	
2e	21.9	1.2	34.9	1.3	23.4	1.8	23.9	2.3	22.1(1)	0.6(2)
3e	19.8	0.7	29.3	1.0	24.8	2.0	21.1	1.9	19.7(1)	0.7(1)
a_2	17.7	0.3	28.9	0.1	25.3	1.0	18.0	1.1	18.8(2)[g]	

(continued....)

Table I (continued)

a) In eV.

b) Relative to the deepest level. Where in SW/CNDO the deepest level is predicted to be an *e* level it is set to be $I_o = 2.0$. Calculations are based on net populations with a σ(C2s): σ(C2p): σ(H1s) cross section ratio of 13 : 1 : 0. For these levels the exact ratios used are not important as long as σ(C2s) ≫ σ(C2p). For the experimental results, the deepest resolvable band is set to $I_o = 1.0$.

c) The level assignments for cyclopentane and cyclohexane are based on the planar ($\mathcal{D}_{5h}$) and chair ($\mathcal{D}_{3d}$) geometries[13] used respectively. The assignments for cycloheptane and cyclooctane are discussed in notes *h* and *i*.

d) Extended Hückel.

e) See ref. 14.

f) See ref. 15.

g) Where *a* levels are very closed to *e* levels, it was necessary to fix their area ratios to those from GAUSS 70 when performing a non-linear least squares fitting program. This enabled good estimates of the energy separation between the *a* and *e* levels.

h) Unlike cyclopentane, which can be considered flat with 108° C-C-C angles, planar cycloheptane would have 128.6° angles and considerable strain. The molecule actually pseudorotates among several forms. The lowest energy form is a twisted chair,[13] which was used for the calculations and has no symmetry. The molecular orbitals can, however, be grouped according to energy and atomic orbital composition into an *a* and three *e* levels and assigned as if the molecule were $\mathcal{D}_{7h}$, as shown.

i) Cyclooctane calculations were performed using the tub geometry, $\mathcal{D}_{2d}$. The b_2 and b_1 levels, which have the same atomic orbital character, are reported as 2*e*. Because the tub form forces four sets of hydrogens within 1.4 Å of each other, the a_2 level is ∿1 eV lower E_B than expected. The intensities, however, are quite insensitive to the precise geometry as long as the C-C distances and angles are constant.

Figure Captions

Fig. 1. Cleaved crystal and amorphous film photoelectron spectra of silicon, germanium, and arsenic taken with monochromatized Aℓ Kα x-rays (1486.6 eV). Binding energy scale is relative to the Fermi level. Bands 1 and 2 are s-like.

Fig. 2. Gas phase photoelectron spectra of cyclopentane, cyclohexane, cycloheptane, and cyclooctane taken with Mg Kα x-rays. The same spectra taken using Aℓ Kα x-rays look identical to these.

Fig. 3. A comparison of the XPS spectra of cyclohexane, diamond, and neopentane [$C(CH_3)_4$]. The energy axis of the diamond spectrum has been shifted to roughly align the peaks with those in cyclohexane. This is the common procedure because gas and solid phase spectra are referenced differently and thus only energy differences can be compared accurately.

Fig. 4. The spectrum of cyclohexane (see Fig. 3) broadened by 0.8 eV and spectra simulating different ring systems (also broadened by 0.08 eV). See text.

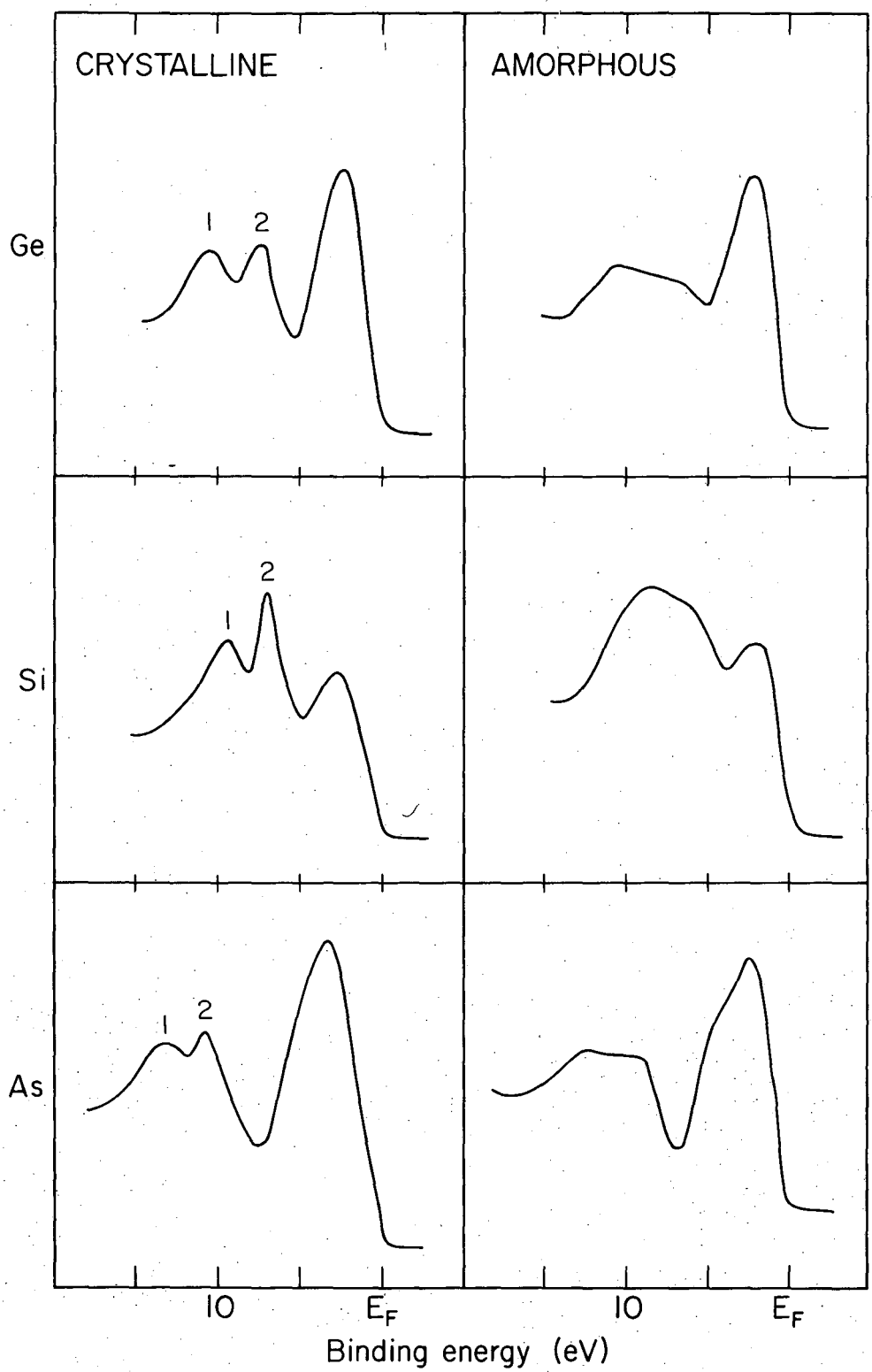
CRYSTALLINE
AMORPHOUS
Ge
Si
As
1
2
10
E_F
Binding energy (eV)
XBL 764-2759

Fig. 1

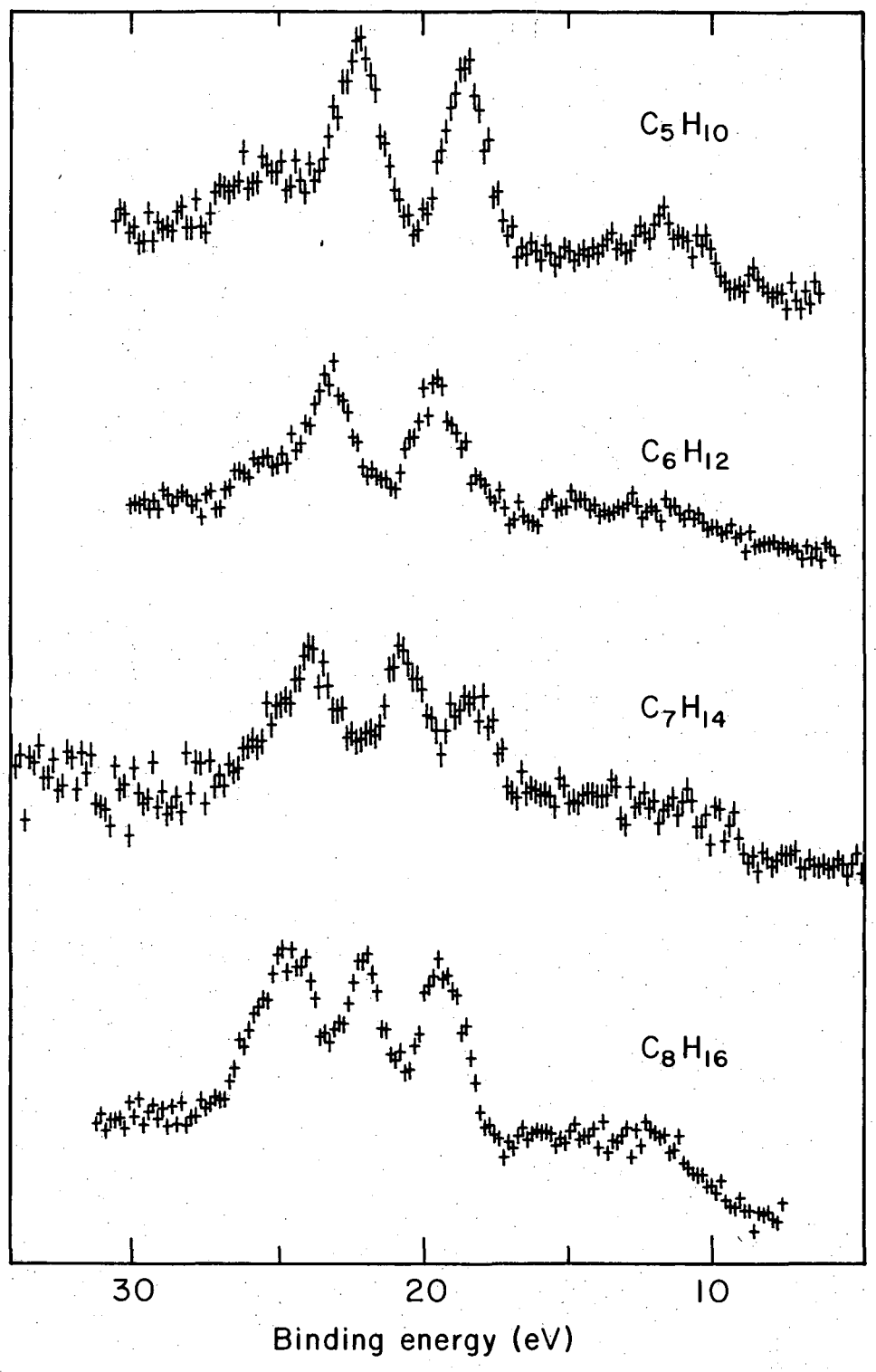

XBL756-3126

Fig. 2

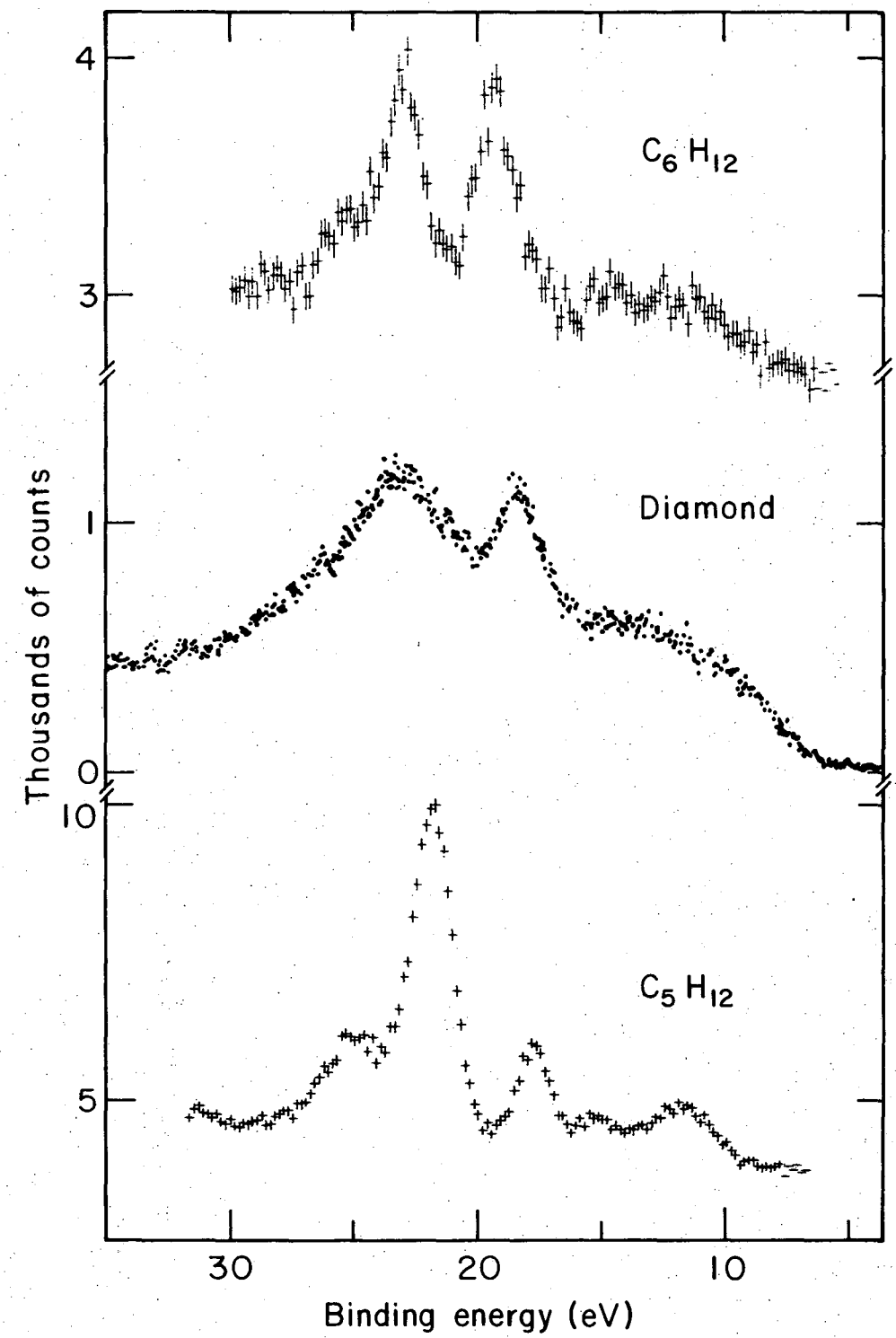
4
3
1
0
10
5
Thousands of counts
$C_6 H_{12}$
Diamond
$C_5 H_{12}$
30
20
10
Binding energy (eV)
XBL756-3127

Fig. 3

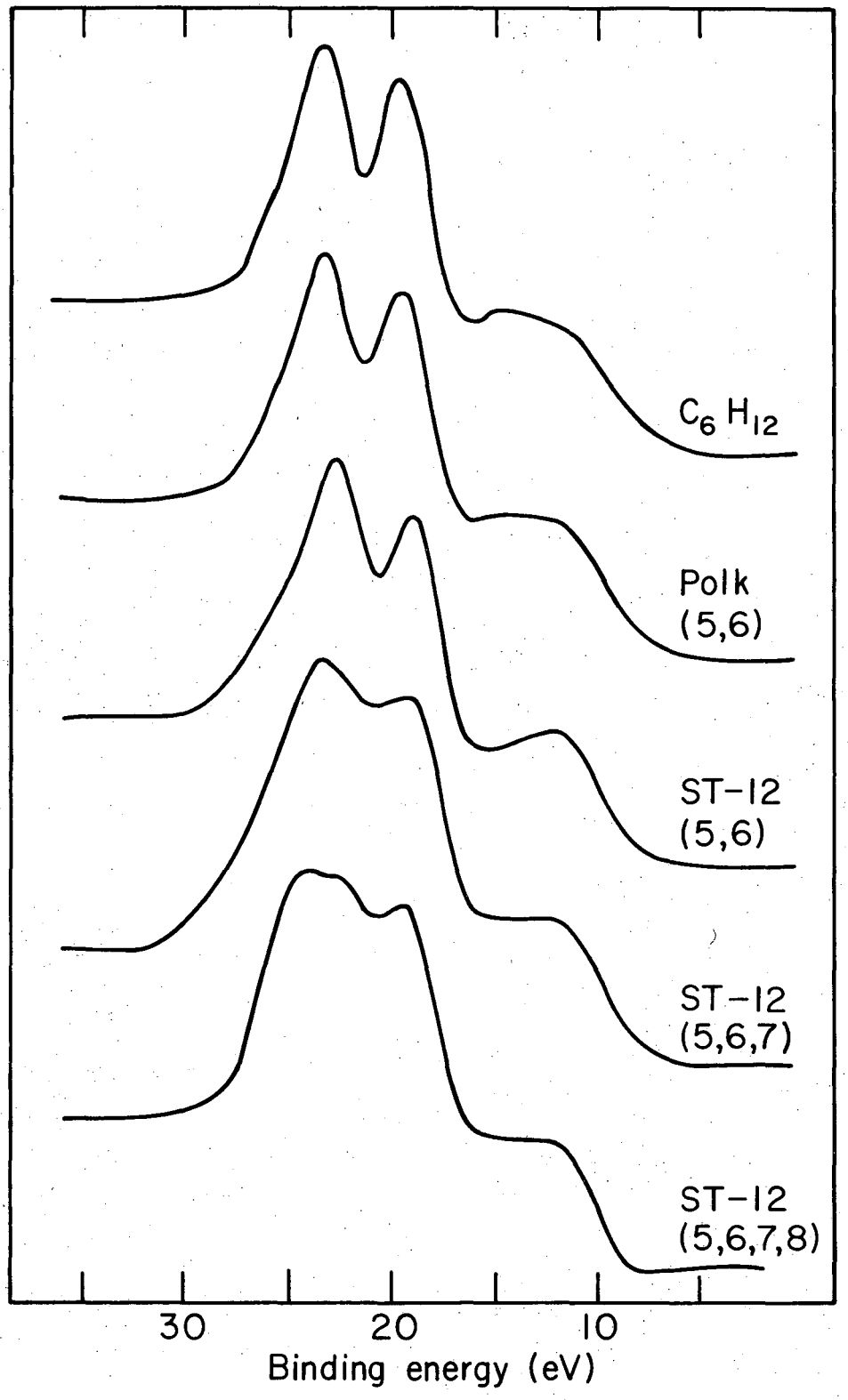

XBL 764-2760

Fig. 4

V. THE FLUORINE 1s CORRELATION-STATE ("SHAKE-UP") SPECTRUM IN THE PHOTOIONIZATION OF HYDROGEN FLUORIDE

Abstract

The x-ray photoemission spectrum of the F 1s region of gaseous HF was measured using Aℓ $K\alpha_{1,2}$ radiation. Several satellite ("shake-up") peaks were observed at ∿25-35 eV higher binding energy than the main F 1s peak. The spectrum was interpreted in terms of a many-electron theory that includes configuration interaction (CI) in both the hole state and the ground state. Of the six excited states predicted to have intensities over 0.1% that of the main peak, the four most intense were clearly present by visual inspection of the spectrum, and all six were readily fitted by the addition of constraints. Derived intensities were in very good agreement with theory if the theory included ground-state CI. The four most intense peaks can be crudely interpreted as arising from $3\sigma \rightarrow 4\sigma$, $1\pi \rightarrow 2\pi$, and $1\pi \rightarrow 3\pi$ excitations.

Introduction

Photoemission spectra of atomic core levels in atoms and molecules yield for each core level j a main peak at an electron kinetic energy

$$K = h\nu - E_B^{(0)} \quad . \tag{1}$$

Here $h\nu$ is the photon energy and $E_B^{(0)}$ is the binding energy of core level j. This main peak corresponds to a special atomic or molecular ion final state. In a single-determinant description, this state would be formed from the ground state by removing an electron from orbital j and allowing the wave functions of the passive electrons to relax adiabatically (i.e., without changing their quantum numbers).

If $h\nu$ is substantially larger than $E_B^{(0)}$, additional weak satellite peaks may also be observed at higher binding energies $E_B^{n'}$. Qualitatively, one usually describes these states as arising from at least a two-electron excitation from the ground state (ionization accompanied by "shake-up"). A quantitative theoretical treatment of the transition cross section to such states, however, shows that one-electron descriptions may be misleading. The cross section for such a transition owes much of its strength to many-body effects. In particular, configuration interaction (CI) in both the initial and final state is required; hence these states are more accurately described as "correlation states", and the satellite peaks in the spectrum as "correlation peaks".

The theoretical formalism for calculating correlation-state spectra was described by Martin and Shirley.[1] The calculations on HF were described by Martin, Mills, and Shirley.[2] In this chapter the fluorine 1s correlation-state spectrum in gaseous HF is compared with

the theory. To our knowledge this is the first case showing quantitative agreement between experiment and theory.

Two major levels of sophistication were used for the wavefunctions reported in ref. 2. First, configuration interaction among the ionic final states was considered, with the ground state represented by a single Slater determinant (Method A). In the next step CI in the ground state was also included (Method B). For each of these cases, the relative intensities of the correlation peaks were computed in the overlap approximation. They are listed in Table I along with calculated energies and experimental energies and intensities.

It was shown in ref. 1 that, for core-level satellites, the dipole and sudden approximations give essentially identical results in the overlap approximation. In ref. 2 an estimate of the variation in the energy-dependent term was obtained assuming the photoelectron continuum function to be represented by a plane wave. This causes the relative intensities calculated from the dipole approximation to decrease slightly and from the energy dependent form of the sudden approximation to increase slightly. Of course, for this to be true the energy of the photoelectron ($\sim$800 eV in this case) must be large compared to the energy variation over the spectrum. These variations are not reflected in Table I since they are less than 3%, well within experimental error.

Experimental

The gaseous sample was obtained by evaporation of 99.9% + pure liquid HF. purchased from Matheson Gas Products, Inc. At 26°C the association constants of HF are:[3]

$$2\ HF \rightleftharpoons (HF)_2 \qquad \log \beta_2 = -3.80 \quad ,$$

$$6\ HF \rightleftharpoons (HF)_6 \qquad \log \beta_6 = -13.94 \quad ,$$

with pressures expressed in torr. Thus oligomerization is unimportant at the pressures of < 1 torr used in this work.

The photoelectron spectra were obtained using Aℓ $K\alpha_{1,2}$ x-rays (1486.6 eV) on the 50 cm radius Berkeley iron-free magnetic spectrometer.[4] Spectral data points were taken at ∿0.4 eV energy increments, at pressures of ∿50 and ∿350 microns (Fig. 1). The analyzer chamber was maintained at a pressure of approximately 10^{-5} torr. The high pressure spectrum was used to determine which of the satellites of the F 1s main line were caused by inelastic electron collisons since the relative intensities of these peaks should increase with pressure. If the low pressure spectrum (Fig. 1b) is subtracted from the high pressure spectrum (Fig. 1a), with appropriate weighting to equalize the main F 1s peaks, the result is an inelastic electron loss spectrum.

The low pressure spectrum was fitted (Fig. 2) using a non-linear least squares program which automatically took into account the (weak) Aℓ $K\alpha_3$ and $K\alpha_4$ components as well as the slight change of the energy window caused by the magnetic spectrometer (which produces spectra linear in momentum, rather than energy). The main peak, corresponding to the F 1s hole state, was fitted best by a sum of three Lorentzian functions and these were used as the fundamental form for the "correlation" peaks.

No attempt was made to locate satellites with intensity 0.1% or less of the main peak. It was necessary to fix the area ratios and

separations of states 7 and 10 relative to their large neighbors (5 and 9, respectively). Theoretical area ratios and separations, described below, were used for these two cases.

Because of the large number of unknowns, the energy positions and full widths at half-maximum (FWHM) of a few peaks were fixed initially, and the fitting program was constrained to vary only the parameters for these remaining. These newly found optimum parameters were then frozen and the rest of the set (those originally fixed) varied. This successive approximation technique was continued until a self-consistent set of parameters was found. The quality of the fit was judged from the statistical χ^2 and visual examination of the plot (Fig. 2).

The results in Table I indicate that the theoretical intensities are in excellent agreement with experiment. Theoretical energies, relative to the main line, are 2.1 to 3.5 eV higher than experiment.[5] For the weaker satellites which are relatively near the double ionization ("shake-off") limit, this excellent agreement is obtained only with a deconvoluted peak which has a very large FWHM. We regard such close agreement with experiment in this region as largely fortuitous. As the shake-off limit is approached, one would expect to begin to observe Rydberg series. Our spectrometer cannot resolve these and our calculations should become progressively less reliable as the limit is approached. Thus both the experimental and theoretical intensities in this region may have rather large error bars. These problems in no way affect the major conclusions of this work.

Conclusions

First and perhaps of most importance, the excellent agreement between experiment and Method B (Table I) provides strong evidence that the over-lap approximation utilizing both initial and final state configuration interaction is adequate to describe such a high-energy core-level correlation-state spectrum. The corollary conclusion is that initial-state CI must be included, since Method A (Table I) gives poor intensity predictions. This is entirely expected in view of the discussion in ref. 1, but has not been recognized in previous work on core level satellite spectra.

We have mentioned that at these energies the energy-dependent factor in the cross section can safely be neglected. At lower photon energies, however, these terms might be expected to become more important. It is difficult to say at what point they would no longer be negligible, and, perhaps more importantly, at what point the plane wave approximation itself becomes poor. Our results, in fact, do not imply that the plane wave approximation is good even at these energies. They simply suggest that the energy dependence--whatever its form--is slowly varying. The usefulness of the plane wave approximation is an important question at the present time since several theoretical models for predicting the intensities or molecular orbital photoemission spectra use either it or a closely related type of continuum function. Further work on this point is in progress in our laboratory.

It is interesting to interpret the correlation peak intensities in terms of a one-electron model--"shake-up" excitation into virtual orbitals. The first two correlation states (1 and 2) can be described

fairly well as arising from the $3\sigma \rightarrow 4\sigma$ transition.[2] These two final states are describable as molecular valence states, the remainder of the spectrum corresponding primarily to Rydberg-like states. Only state 2 of this pair is predicted to have an observable intensity, and it is indeed the first state observed in the experimental spectrum. It seems reasonable to assert that the relatively low intensity of this transition is attributable to the charge transfer nature of the excitation. The 3σ orbital is the bonding combination of the F(2p) and H(1s) orbitals and is largely localized on the fluorine atoms, while the 4σ is the anti-bonding combination and is primarily hydrogen-like. Since the orbitals have their large components in different regions of space, one would expect a small overlap. This interpretation seems plausible, but there are also more subtle effects that contribute substantially to the cross section. These are the small admixture of the $1\pi \rightarrow 2\pi$ excitation into state 2, the even smaller admixture of the reference state, and the effect of configuration interaction in the initial state. This last point is very important and can be seen quite clearly in Table I. The inclusion of initial state CI (Method B) nearly doubles the predicted intensity of state 2 relative to the primary hole state.

The most intense peak in the spectrum, state 5, corresponds to the $1\pi \rightarrow 2\pi$, or $F(2p_\pi) \rightarrow F(3p_\pi)$ excitation. Its counterpart, state 3, is also relatively intense. The next most intense peak in the spectrum is state 9, the $F(2p_\pi) \rightarrow F(4p_\pi)$ excitation. These results, of course, would be expected on the basis of a simple one-electron overlap model.

Satellites with smaller intensities are less predictable. State 7 is primarily attributable to the $3\sigma \rightarrow 5\sigma$ excitation. It would be

tempting to say that since the 5σ orbital is F(3s)-like, there should be very little overlap with the 3σ orbital in the ground state (which is mainly $F(2p_\sigma)$-like), and this causes the small intensity of state 7. These arguments, however, are probably oversimplified since there is a fairly large component of $3\sigma \rightarrow 6\sigma$ ($F2p_\sigma \rightarrow F3p_\sigma$) in the wave function. Configuration mixing makes it nearly impossible to give rough *a priori* estimates of intensities. For example, the $3\sigma \rightarrow 6\sigma$ excitation is important in state 8, and it might therefore be expected to be rather intense. It is not. The $F(2p_\sigma) \rightarrow F(4s)$ excitation, state 10, on the other hand, has a much larger intensity. The reasons for these differences in overlap are complex, and are tied into the specific nature of configuration mixing in these excited states. Since the configurations enter into the wave function with a phase, they can either add intensity to the predominant configuration, or cancel what intensity the dominant configuration might supply. These problems are expected to be more severe in molecules than atoms since there is generally a much denser excited-state manifold in the molecular species.

Finally, we note that the HF molecule is ioselectronic with the Neon atom. One might therefore expect to see some similarities in their satallite spectra. In Figs. 3a and 3b we have drawn a bar spectrum of the most intense satellites in Ne[6] and HF. Above each bar we have assigned an orbital which serves to roughly identify the final state.

The most intense satellites in the Ne 1s spectrum are derived from $2p \rightarrow np$ excitations. If one imagines the two nuclei in HF being adiabatically compressed into a united atom, the 3σ and 1π orbitals

of the molecule correlate with Ne 2p while 4σ and 2π correlate with the Neon 3p orbital. Since the major intensity in neon comes from the $2p \rightarrow 3p$ excitation, it is not surprising that the most intense peaks in HF arise from the $3\sigma \rightarrow 4\sigma$ and $1\pi \rightarrow 2\pi$ excitations. The $(1\pi \rightarrow 4\pi)$ state in HF is also relatively intense and correlates with the $2p \rightarrow 4p$ excitation in the united atom.

Another qualitatively interesting comparison is to consider the "equivalent cores" analog of the F 1s hole state is HF, i.e., the species $(NeH)^+$. The charge distribution in this system is presumably intermediate in character between the two extremes $Ne - H^+$ and $Ne^+ - H$, with the latter ($:\ddot{N}e:H$) being the more chemically reasonable. The correlation states of HF might thus be expected to be similar to the excited states of Ne^+. The states of Ne^+ derived from $2p \rightarrow 3p$ excitations[7] are shown diagramatically in Fig. 3c. They have been given intensities based on the total degeneracy of each state. This simple picture seems to work quite well, as can be seen by comparing Fig. 3c to Fig. 3b. Although no detailed correlation between specific states can be drawn, this model reproduces the observed shift in HF vs. Ne toward smaller satellite separation from the primary state.

In summary, the correlation-peak spectrum of HF can be calculated quite satisfactorily in the overlap approximation. The intensities of the correlation peaks are very dependent upon the effects of configuration interaction in both the initial and final states. At present, quantitative prediction of such spectra based on simple one-electron models seem doomed to failure. Even qualitative estimates and assignments are very difficult considering the importance of configuration

interaction in the final state. The effect of CI in the initial state is to increase the intensities of the shake-up states at the expense of the primary hole state. For HF, the shake-up states are all roughly twice as intense once initial state CI is included. This increase in intensity is obviouly necessary to reproduce the experimental spectrum.

References

1. R. L. Martin and D. A. Shirley, to be published in J. Chem. Phys., 1976.

2. R. L. Martin, B. E. Mills, and D. A. Shirley, to be published in J. Chem. Phys., 1976.

3. J. N. Maclean, F. J. C. Rossotti, and H. S. Rossotti, J. Inorg. Nucl. Chem. 24, 1549 (1962).

4. For further details see: D. W. Davis, D. A. Shirley, and T. D. Thomas, J. Amer. Chem. Soc. 94, 6565 (1972).

5. The reason the energies are consistently higher than experiment is that the orbital basis used in the CI expansion was optimized for the primary hole state, not the correlation states.

6. K. Siegbahn, C. Nordling, G. Johansson, J. Hedman, P. F. Hedén, K. Hamrin, U. Gelius, T. Bergmark, L. O. Werme, R. Manne, and Y. Baer, ESCA Applied to Free Molecules (North-Holland, Amsterdam, 1969).

7. C. E. Moore, Atomic Energy Levels, NBS Circ. 467, Washington, 1949.

Table I. Correlation Peak Intensities in the Overlap Approximation

State[a]	I (theo)[b] Method A	I (theo)[b] Method B	I(expt)[c]	FWHM (eV)	E(theo)[d] (eV)	E(expt)[d] (eV)
0	(1.000)	(1.000)	(1.000)	1.4	(693.5)	(694.0(5))
1	0.000	0.001	–	–	23.89	
2	0.012	0.020	0.019(3)	2.1(3)	25.90	22.4(2)
3	0.015	0.030	0.030(4)	2.3(3)	29.57	26.50(9)
4	0.000	0.000	–	–	30.89	–
5	0.036	0.062	0.057(5)	3.7(3)	32.35	29.90(7)
6	0.000	0.001	–	–	32.72	–
7	0.007	0.012	0.010	4.7(3)	33.31	30.87
8	0.000	0.000	–	–	33.74	–
9	0.028	0.041	0.038(5)	7.1(9)	34.84	32.7(3)
10	0.005	0.007	0.007	7.9(9)	35.43	33.3
11	0.000	0.000	–	–	35.72	–

a) In order of increasing energy. "Reference state" is numbered 0, as in Fig. 1 and text.

b) All intensities normalized to peak 0. Absolute values of the overlap integral in state 0 are 0.78115 (Method A), 0.71970 (Method B).

c) Error in last place given parenthetically.

d) First entry is the absolute binding energy of the reference state; the others are incremental energies relative to this.

Figure Captions

Fig. 1. a) High pressure and b) low-pressure photoelectron spectra of the F 1s region in HF using Aℓ $K\alpha_{1,2}$ x-rays. The scale for the correlation and inelastic loss peaks is expanded 20 times that for the main peak.

Fig. 2. Correlation peaks of HF F 1s relative to the main line along with the computer fit (see Table I and text). The crosses represent actual data points; the circles represent data corrected for the inelastic energy loss peak at about 20 eV.

Fig. 3. a) The most intense satellites of the Ne 1s hole state. The correlation of these states with the HF satellites is shown by the dotted lines.

b) The most intense states of the HF satellite spectrum. The abscissa is the separation from the primary state and the ordinate is the intensity relative to the primary state. Above each bar an orbital designation is provided which roughly identifies the final state (see text).

c) The excited states derived from the configuration $1s^2 2s^2 2p^4 3p$ of the Ne^+ ion. They have been given intensities based on the total degeneracy of each state.

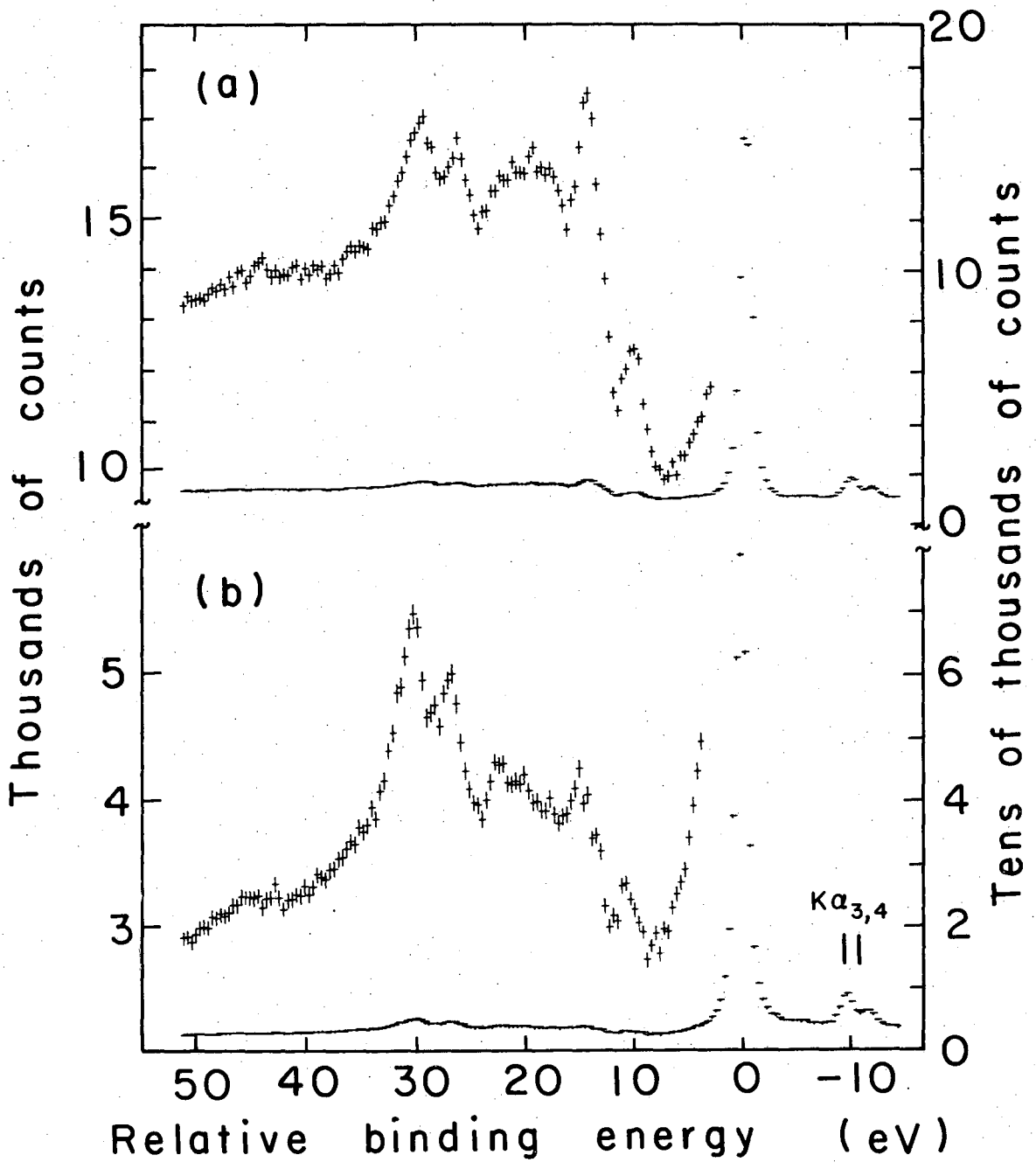

Fig. 1

XBL 752-166

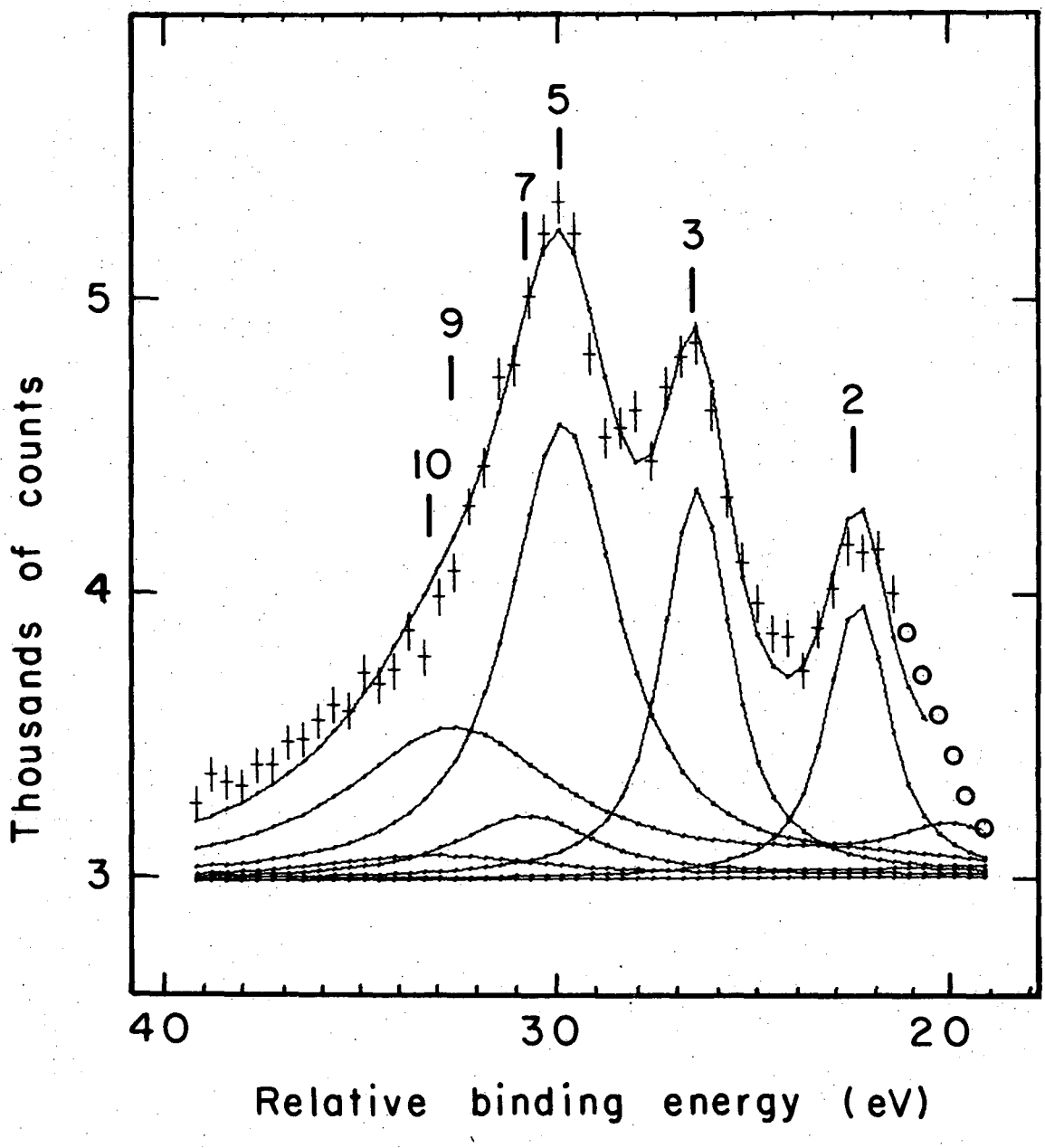

Fig. 2

XBL7412-8360

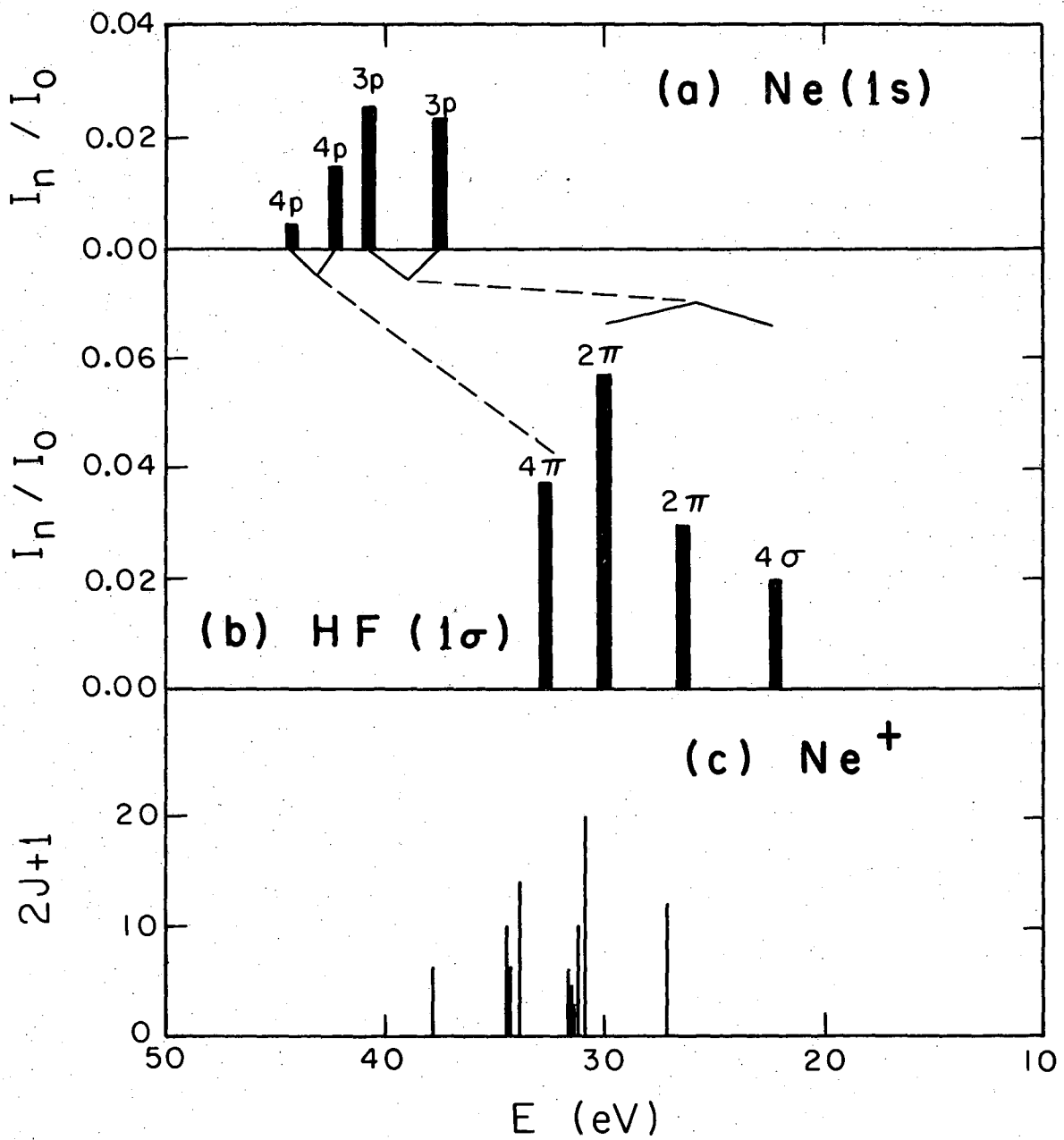

Fig. 3

XBL752-2269

VI. K-SHELL CORRELATION-STATE ("SHAKE-UP") SPECTRA IN FORMAMIDE

Abstract

Carbon, nitrogen, and oxygen K-shell correlation-state spectra give detailed qualitative confirmations of predictions by Basch. This prototypical study, with 1s holes on three different elements, shows that $\pi \rightarrow \pi^*$ excitations are differentially stabilized according to the location of the 1s hole.

Basch has recently performed multi-configuration self consistent field calculations with configuration interaction on the ground state and certain hole states of formamide.[1] From these he predicted the relative positions and intensities of the correlation-state or "shake-up" peaks accompanying photoionization of K electrons from carbon, nitrogen, and oxygen. The outermost three filled orbitals of planar formamide are described as $\pi_1^2 n^2 \pi_2^2$, while the lowest unoccupied orbital is π_3. Basch compared trends in shake-up states corresponding to the excitations $\pi_2 \rightarrow \pi_3^*$, $\pi_1 \rightarrow \pi_3^*$, and $n \rightarrow \sigma^*$ for K shell photoionization from C, N, and O, making qualitative arguments for the calculated variations. The intuitive appeal of these arguments makes an experimental tests of the predicted trends very desirable. Their confirmation would provide evidence that correlation-state spectra are well enough understood to be used diagnostically. If this should prove to be the case, it may prove possible to use K-shell holes as "test charges" at different points in the molecule. The response of the outer molecular orbitals to these test charges, as clearly manifest in correlation state peak energies and intensities, could provide insight into the dynamics of electronic distributions during chemical reactions.

In order to compare Basch's calculations with experiment we have taken the XPS spectra of the carbon, nitrogen, and oxygen cores in formamide. The liquid was transferred to a glass bulb in a nitrogen atmosphere, then distilled under vacuum into the sample chamber to remove any trace of water. Mg Kα x-rays (1253.6 eV) were used to irradiate the vapor (at 3×10^{-2} torr) above the room temperature liquid.

The electron spectra (shown in Fig. 1) were measured on the Berkeley 50 cm radius magnetic spectrometer with data points ∿0.1 eV apart. To determine whether any of the peaks arise from electron energy loss tue to inelastic scattering, a gold foil was placed in the x-ray beam with formamide vapor between the gold and the entrance slit to the anlayzer. Comparison of a gold 4f spectrum taken in this manner to a spectrum of gold with no formamide present shows a small extra peak at 7.6 eV lower kinetic energy, with 2% the relative intensity of each Au(4f) peak. An electron loss peak would be expected at about this energy because the lowest $\pi \rightarrow \pi^*$ transition in the vacuum ultraviolet spectrum of formamide falls in a series of bands centered at 7.5 eV with a width of about 1 eV.[2] Presumably this is the $\pi_2 \rightarrow \pi_3^*$ transition. In interpreting our K-level satellite spectra we allowed for this loss peak. It can account for the first weak satellite in the N(1s) spectrum but only for a small fraction of the 7.4 eV oxygen satellite. In the carbon spectrum it appears as a slight shoulder on the 9.5 eV peak.

Basch noted that the π_1, π_2, and π_3 molecular orbitals (MO's) differ significantly in their distribution of atomic pπ character. The π_1 orbital is roughly equally distributed over C, N, and O 2p atomic orbitals. In the π_2 MO the carbon atomic character is very small, but the π_3 MO is more concentrated on the carbon atom, with smaller and nearly equal admixtures of nitrogen and oxygen functions. A K hole on a given atom will stabilize orbitals that are concentrated on that atom. Thus Basch predicted that the $\pi_2 \rightarrow \pi_3^*$ energy difference would be lower in the C(1s) satellite spectrum than in normal formamide,

while in the N(1s) and O(1s) spectra the energy of the transition would be increased. Basch's calculations bore this prediction out theoretically, as indicated in Table I.

The experimental spectra provide strong support for these predictions. Although all three spectra show satellites between 7 and 10 eV, the satellite so dominates the spectrum in the C(1s) case that we feel it should be assigned to the $\pi_1 \rightarrow \pi_3^*$ transition, which is predicted to lie at 10.1 eV with 8.3% intensity. There is no spectral feature that can be positively identified as a peak in the C(1s) spectrum between the main peak and this intense $\pi_1 \rightarrow \pi_3^*$ satellite, which lies at 9.6 eV relative energy and has an intensity of 7.2%. The small excursion at 5 eV is too narrow to be a true peak. It is not reproducible as such a well-defined peak, but there appears to be some spectral area at this energy. This would be consistent with the predicted $\pi_2 \rightarrow \pi_3^*$ peaks of 0.36% and 0.45% intensities, at 3.26 eV and 6.45 eV, respectively. The limited statistical accuracy of this experiment and the possibility of interference by Mg $K\alpha_{3,4}$ satellites of the peak at 13.8 eV combine to preclude a definite assignment, however.

The 9.9 eV peak of 3.5% intensity in the N(1s) spectrum fits well with the predicted values of 10.32 eV and 4.57% for the $\pi_2 \rightarrow \pi_3^*$ transition. In the O(1s) case the 7.4 eV, 7.3% peak falls at a lower energy and shows less intensity than the prediction (9.13 eV, 16.81%), but the predicted trend in intensity is qualitatively borne out.

For the C(1s) and O(1s) spectra the next correlation states are expected to arise through the $\pi_1 \rightarrow \pi_3^*$ excitation. K holes on C, N, or O would stabilize the π_1 orbital by similar amounts because this orbital

is distributed rather equally on the three atoms. The concentration of the π_3 orbital on carbon implies that a K hole on carbon will stabilize this orbital more than would a nitrogen or oxygen K hole. Thus the $\pi_1 \rightarrow \pi_3^*$ transition energy should be lower in the C(1s) spectrum than in that of N(1s) or O(1s). The experimental spectra are consistent with this picture. The $\pi_1 \rightarrow \pi_3^*$ peak is predicted to lie at 10.1 eV in the C(1s) spectrum, with 8.3% intensity. We interpret the observed peak at 9.6 eV, with 7.2% intensity, as the $\pi_1 \rightarrow \pi_3^*$ peak. In the O(1s) spectrum the second large satellite, at 13.9 eV with 8.5% intensity, fits the predicted parameters (15.4 eV, 8.1% intensity) very well: We assign this peak to the $\pi_1 \rightarrow \pi_3^*$ transition.

The $\pi_1 \rightarrow \pi_3^*$ state in the N(1s) spectrum was predicted to lie at a higher energy than the $n \rightarrow \sigma^*$ peak, and no intensity was predicted. One of the most intense peaks in the N(1s) spectrum (5% intensity) is the most likely candidate for the $\pi_1 \rightarrow \pi_3^*$ transition.

Finally, some predictions were made for the $n \rightarrow \sigma^*$ state. A peak from this state was predicted to lie at 12.4 eV in the N(1s) spectrum with an intensity of 1.76%. There is a shoulder at $\sim$12.8 eV in the spectrum, with $\sim$1.7% intensity. The C(1s) spectrum shows a well-resolved peak at 13.8 eV with 1.8% intensity, while the theoretical predictions are 13.8 eV and 0.5% intensity. In the O(1s) case there is a small peak at 20.6 eV with 1% intensity. This may be the $n \rightarrow \sigma^*$ state, which was predicted at 19.2 eV (no intensity was predicted). All three of these $n \rightarrow \sigma^*$ assignments are really only suggestions, both because the theoretical work is incomplete and because the spectra all show very broad features peaking near 20 eV.

These broad features are of some interest. Integration over their total areas would yield the total correlation-state (or "shake-up") intensities, if it were feasible to ascertain reliably what fractions of their areas arise from intrinsic effects, as distinguished from inelastic energy loss. Unfortunately, the intensities available with our spectrometer precluded the pressure-dependence studies that would yield this information. Indirect evidence, the return of the intensity to the baseline at 40-50 eV, analysis of the Au(4f) photoelectron loss spectrum in formamide, and comparison with correlation-state studies in other molecules--indicates that most of the spectral area does, in fact, arise from intrinsic effects. The total integrated area up to 50 eV is 40% of the main peak area in carbon, 41% in nitrogen, and 50% in oxygen. This corresponds to total probabilities for multiple excitation (P_M) of 0.29 (C 1s), 0.29 (N 1s), and 0.33 (O 1s).[3] Basch did not calculate P_M in these three cases, but we may infer from his results that it is large. By comparison, Bagus, et al.[4] calculated $P_M = 0.42$ for an oxygen 1s hole in O_2, and P_M(N 1s) = 0.25, P_M(O 1s) = 0.28 in NO.

A graphical summary of the principal results of this work is given in Fig. 2. Only the $\pi \rightarrow \pi^*$ excitations are included. Basch's calculation provided the incentive for these measurements and were used extensively in their interpretation. Further calculations and experiments, when they become feasible, are clearly desirable. Nevertheless the detailed agreement of experiment with theory is very encouraging at this stage. This agreement indicates that correlation-state spectra can be used to determine the responses of individual

molecular orbitals to "test charges"--1s holes--on individual atoms.

References

1. Harold Basch, Satellite Bands and the Ion States of Formamide, to be published.

2. H. D. Hunt and W. T. Simpson, J. Amer. Chem. Soc. 75, 4540 (1953).

3. We emphasize that these values are really upper limits, for reasons given above.

4. P. S. Bagus, M. Schrenk, D. W. Davis, and D. A. Shirley, Phys. Rev. A 9, 1090 (1974).

Table I. Comparison of Theoretical and Experimental K-Shell Correlation-State Spectra in Formamide

	Carbon				Nitrogen				Oxygen			
	Theory		Expt.		Theory		Expt.		Theory		Expt.	
	ΔE[a]	I[b]	ΔE	I	ΔE	I	ΔE	I	ΔE	I	ΔE	I
(Main Peak)	0	100	0	100	0	100	0	100	0	100	0	100
$\pi_2 \rightarrow \pi_3^*$	3.26	0.36	5?	<0.5	5.32	0.01	9.9(2)	3.5(7)	5.87	0.01	7.4(1)	7.3(4)[e]
	6.45	0.45			10.32	4.57			9.13	16.81		
$\pi_1 \rightarrow \pi_3^*$	8.98	0.09	9.6(2)[e]	7.2(4)[c]	15.66	*d*	15.0(2)	5.0(8)	13.72	0.79	13.9(3)	8.5(5)
	10.10	8.33			17.06	*d*			15.37	8.11		
$n \rightarrow \sigma^*$	12.53	0.10	13.8(2)[e]	1.8(3)[e]	11.70	0.90	12.8(4)[e]	1.7(7)[e]	19.21	*d*	20.6(3)[e]	1.0(5)[e]
	13.81	0.50			12.38	1.76						

[a] Energies in eV.

[b] Intensities are given as percentage of main peak intensities. The error arises partly from the uncertainty in the base line which was drawn with consideration for the broad band centered at about 22 eV.

[c] After correction for 2% of main peak intensity arising from 7.5 eV inelastic energy loss peak (see text).

[d] Not calculated.

[e] The interpretation of $n \rightarrow \sigma^*$ features is highly tentative (see text).

Figure Captions

Fig. 1. Correlation-state spectra of the C(1s), N(1s), and O(1s) hole states in gaseous formamide at room temperature and 3×10^{-2} torr pressure, excited by Mg Kα radiation. The right scale refers to the complete spectrum; the left, to the expanded spectrum.

Fig. 2. Systematic variations of $\pi_2 \rightarrow \pi_3^*$ and $\pi_1 \rightarrow \pi_3^*$ excitation energies and intensities in gaseous formamide. Where available, intensities are denoted by (horizontal) lengths of wide bars: open figures denote calculated values, filled figures, experimental results. The low excitation energies accompanying C(1s) ionization are attributed to stabilization of the π_3 orbital, which is largely C(2p) in character, by the (positive) hole.

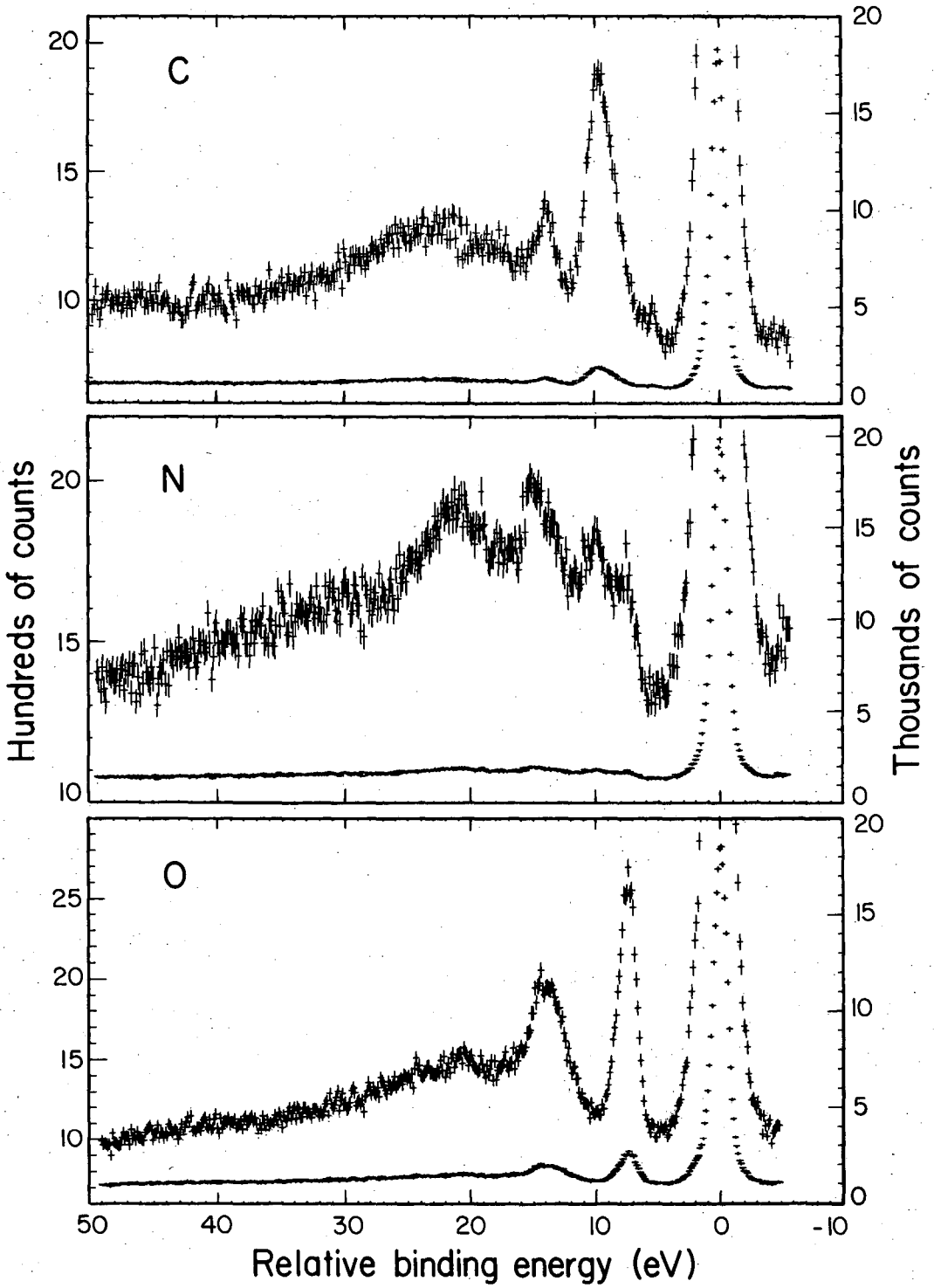

XBL 7511-9555

Fig. 1

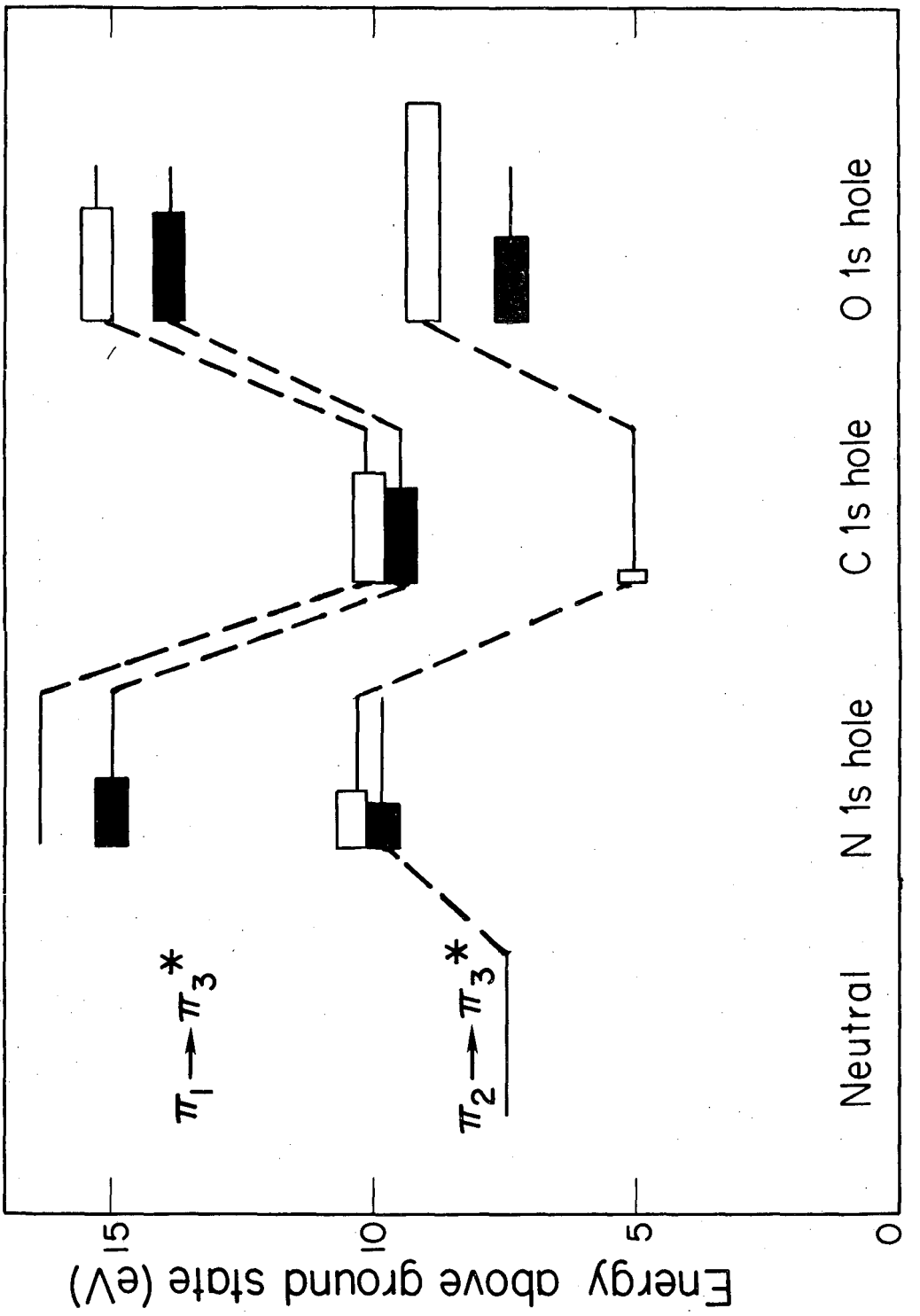

Fig. 2

ACKNOWLEDGEMENTS

I am very grateful to Professor David A. Shirley for his guidance and support.

This work was done with support from the U.S. Energy Research and Development Administration. Any conclusions or opinions expressed in this report represent solely those of the author and not necessarily those of the Lawrence Berkeley Laboratory nor of the U.S. Energy Research and Development Administration.

TECHNICAL INFORMATION DIVISION
LAWRENCE BERKELEY LABORATORY
UNIVERSITY OF CALIFORNIA
BERKELEY, CALIFORNIA 94720